MFI of Tim-3 or PD-1 within $CD4^+$ or $CD8^+$ cells (data not shown). The percentage of infected $CD4^+$ and $CD8^+$ cells in asymptomatic carriers or $tetramer^+CD8^+$ cells in HAM/TSP patients was too small to assess Tim-3 or PD-1 expression.

CONCLUSIONS

We found that the proportion of $Tim\text{-}3^+$ cells within $CD4^+$ and $CD8^+$ T cell populations of HTLV-I–infected individuals (both HAM/TSP patients and asymptomatic carriers) is significantly lower than in healthy controls (Figure 1). This reduction was much clearer in Tax-specific CTLs because the frequency of Tim-3–expressing cells in CTLs was lower than in the total $CD8^+$ population of infected individuals (Figures 2*B–D*). In addition, $Tim\text{-}3^+$ cell frequency in HTLV-I Tax-specific CTLs was significantly lower than in CMV-specific CTLs from HAM/TSP patients (Figure 2*B*). Interaction of Tim-3 with its ligand, galectin-9, regulates Th1 cell responses by promoting the death of IFN-γ–producing Th1 cells, suggesting that Tim-3 may play a role in suppressing Th1-mediated immune responses [18]. Our results showing that the frequency of $Tim\text{-}3^+$ cells is reduced within $CD4^+$ and $CD8^+$ T cells in HTLV-I infection strongly suggest that the Th1/Tc1 immune response is not negatively regulated by Tim-3 in HTLV-I infection. Rather, immune cells such as HTLV-I–specific CTLs may be resistant to cell death through the Tim-3/galectin-9 pathway [18]. In this sense, the increased number of $Tim\text{-}3^-$ HTLV-I Tax-specific CTLs may contribute to the control of viral replication. In the present study, we found that IFN-γ production was decreased in $CD8^+$ cells and HTLV-I Tax-specific CTLs that expressed Tim-3 as compared with their $Tim\text{-}3^-$ counterparts in HAM/TSP patients (Figure 4). In addition, CD107a expression was lower in $Tim\text{-}3^+$ HTLV-I Tax-specific CTLs from HAM/TSP patients (Figure 5). These results indicate that Tim-3 identifies a subset of CTLs with impaired production of cytokines and cytolytic activity. The decreased expression of Tim-3 in HTLV-I infection is in marked contrast to other chronic viral infections such as HIV and HCV infections, where Tim-3 expression is increased in T cells, including the virus-specific CTLs [19, 20]. It would be of interest to determine whether Tim-3 expression is also reduced in other chronic viral infections and to clarify the mechanisms underlying Tim-3 down-regulation in HTLV-I infection.

Interestingly, our data demonstrated that Tim-3 and CD107a expression in HTLV-I Tax-specific CTLs was not significantly different between HAM/TSP patients and asymptomatic carriers (Figures 2*F* and 5*D*); however, Tim-3 MFI was higher in asymptomatic carriers than in HAM/TSP patients. Our data suggest that the killing activity of the CTLs is not different between the 2 groups. Controversially, others have reported that CD107a expression is lower in HTLV-I Tax-specific CTLs from HAM/TSP patients than from asymptomatic carriers, and that CTL function is impaired in HAM/TSP patients as compared with asymptomatic carriers [24]. This controversy may result from differences in sample type and procedures, including the gating for $tetramer^+$ cells after antigen stimulation. To address this issue, more detailed analyses of HTLV-I–specific CTL function in HAM/TSP patients and asymptomatic carriers would be necessary to ascertain whether differences could define the clinical condition.

In this study, we found that PD-1 expression levels on T cells of HAM/TSP patients and asymptomatic carriers were not different from those of healthy controls. However, we observed that PD-1 expression was significantly higher in HTLV-I Tax-specific CTLs than in CMV-specific CTLs (Figure 3*E*) and significantly higher in HTLV-I Tax-specific CTLs from asymptomatic carriers than from HAM/TSP patients. This result is in partial agreement with a previous study on HTLV-I infection, in which a marked increase of PD-1 expression was found in HTLV-I Tax-specific CTLs from both asymptomatic carriers and ATL patients as compared with CMV- and EBV-specific CTLs [31]. We found that IFN-γ production was higher in $CD8^+$ cells and HTLV-I Tax-specific CTLs that expressed PD-1 as compared with their $PD\text{-}1^-$ counterparts in HAM/TSP patients (Figures 4*E* and 4*F*). In addition, CD107a expression was higher in $PD\text{-}1^+$ HTLV-I Tax-specific CTLs of HAM/TSP patients (Figure 5*C*). These results indicate that $PD\text{-}1^+$ HTLV-I Tax-specific CTLs are capable of producing proinflammatory cytokines and have high cytolytic activity during HTLV-I infection. An increase in IFN-γ production by $PD\text{-}1^+$ T cells has been recently shown in simian immunodeficiency virus (SIV) infection and in an animal model of autoimmune nephritis [32, 33]. Interestingly, $PD\text{-}1^+$ cells were predominantly detected within $CD107a^+$ antigen-specific T cells in SIV infection [34]. In this context, it is proposed that the primary mechanism by which PD-1 affects $CD8^+$ T cell function involves regulation of cell proliferation and survival [32, 35]. Our results suggest that HTLV-I Tax-specific CTLs exhibit an increased expression of PD-1, albeit a reduced expression of Tim-3. This is in marked contrast to other chronic viral infections such as HIV and HCV infections, in which both PD-1 and Tim-3 are expressed at high levels in the virus-specific CTLs [19, 20]. Double staining for Tim-3 and PD-1 revealed that these are expressed by distinct populations of $CD8^+$ T cells in HIV infection and that the predominance of either $Tim\text{-}3^+PD\text{-}1^-$ or $Tim\text{-}3^-PD\text{-}1^+$ cells in HIV-specific CTLs differs among individuals [19]. At the same time, CMV- and HCV-specific CTLs are predominantly $Tim\text{-}3^-PD\text{-}1^+$ and $Tim\text{-}3^+PD\text{-}1^+$, respectively [20]. In our study, the average percentage of $PD\text{-}1^+$ cells in HTLV-I Tax-specific CTLs was 65.9% and 22.3% in carriers and HAM/TSP patients, respectively (Figure 3*C*); the average percentage of $Tim\text{-}3^+$ cells was 3.5% and 3.2%, respectively (Figure 2*F*), suggesting that the majority of the CTLs expressing T cell exhaustion molecules has a $Tim\text{-}3^-PD\text{-}1^+$ phenotype. Taken together, these results suggest that PD-1 and Tim-3 may have a distinct function in regulating immune responses in HTLV-1 infection.

We observed that HTLV-I Tax-expressing cells show a significant reduction in Tim-3 expression as compared with $Tax^{-}CD4^{+}$ cells and that Tim-3 expression in $Tax^{+}CD8^{+}$ cells tends to be lower than in $Tax^{-}CD8^{+}$ cells. $Tax^{+}CD8^{+}$ cells also showed significantly lower PD-1 expression (Figure 6). This suggests that HTLV-I–infected cells may be resistant to cell death through the Tim-3/galectin-9 pathway. HTLV-I Tax combines a positive effect on cell cycle with a negative effect on apoptosis through transactivation of several host genes [36]. It would be of interest to further investigate whether Tax might regulate Tim-3 expression.

In summary, we demonstrated that the expression of the negative immune regulator Tim-3, but not of PD-1, is reduced on HTLV-I Tax-specific CTLs, $CD4^{+}$, and $CD8^{+}$ T cells in both HAM/TSP patients and asymptomatic carriers. Moreover, we showed that Tim-3^{+}, but not PD-1^{+}, cells produce less IFN-γ and exhibit low cytolytic activity within the CTL population. Tim-3 expression and CTL cytolytic activity were not different between HAM/TSP patients and asymptomatic carriers. In addition, $CD4^{+}$ HTLV-I Tax-expressing cells showed a significant reduction in Tim-3 expression as compared with $Tax^{-}CD4^{+}$ cells. These results suggest that HTLV-I Tax-specific CTLs preserve their cytolytic activity, thereby controlling viral replication.

Funding

Grant-in-Aid for Research on Brain Science from the Ministry of Health, Labor and Welfare, Japan, and Grant-in-Aid for Scientific Research from the Ministry of Education, Culture, Sports, Science and Technology, Japan.

Acknowledgments

We thank Ms. Takako Inoue for the excellent technical assistance.

References

1. Richardson JH, Edwards AJ, Cruickshank JK, Rudge P, Dalgleish AG. In vivo cellular tropism of human T-cell leukemia virus type 1. J Virol **1990**; 64:5682–7.
2. Uchiyama T, Yodoi J, Sagawa K, Takatsuki K, Uchino H. Adult T-cell leukemia: clinical and hematologic features of 16 cases. Blood **1977**; 50:481–92.
3. Gessain A, Barin F, Vernant JC, et al. Antibodies to human T-lymphotropic virus type-I in patients with tropical spastic paraparesis. Lancet **1985**; 2:407–10.
4. Osame M, Usuku K, Izumo S, et al. HTLV-I associated myelopathy, a new clinical entity. Lancet **1986**; 1:1031–2.
5. Umehara F, Izumo S, Nakagawa M, et al. Immunocytochemical analysis of the cellular infiltrate in the spinal cord lesions in HTLV-I-associated myelopathy. J Neuropathol Exp Neurol **1993**; 52:424–30.
6. Osame M, Matsumoto M, Usuku K, et al. Chronic progressive myelopathy associated with elevated antibodies to human T-lymphotropic virus type I and adult T-cell leukemialike cells. Ann Neurol **1987**; 21:117–22.
7. Nagai M, Usuku K, Matsumoto W, et al. Analysis of HTLV-I proviral load in 202 HAM/TSP patients and 243 asymptomatic HTLV-I carriers: high proviral load strongly predisposes to HAM/TSP. J Neurovirol **1998**; 4:586–93.
8. Jacobson S, Shida H, McFarlin DE, Fauci AS, Koenig S. Circulating CD8+ cytotoxic T lymphocytes specific for HTLV-I pX in patients with HTLV-I associated neurological disease. Nature **1990**; 348:245–8.
9. Greten TF, Slansky JE, Kubota R, et al. Direct visualization of antigen-specific T cells: HTLV-1 Tax11-19–specific CD8(+) T cells are activated in peripheral blood and accumulate in cerebrospinal fluid from HAM/TSP patients. Proc Natl Acad Sci USA **1998**; 95:7568–73.
10. Bangham CR, Osame M. Cellular immune response to HTLV-1. Oncogene **2005**; 24:6035–46.
11. Blank C, Mackensen A. Contribution of the PD-L1/PD-1 pathway to T-cell exhaustion: an update on implications for chronic infections and tumor evasion. Cancer Immunol Immunother **2007**; 56:739–45.
12. Sharpe AH, Wherry EJ, Ahmed R, Freeman GJ. The function of programmed cell death 1 and its ligands in regulating autoimmunity and infection. Nat Immunol **2007**; 8:239–45.
13. Okazaki T, Honjo T. Rejuvenating exhausted T cells during chronic viral infection. Cell **2006**; 124:459–61.
14. Barber DL, Wherry EJ, Masopust D, et al. Restoring function in exhausted CD8 T cells during chronic viral infection. Nature **2006**; 439:682–7.
15. Trautmann L, Janbazian L, Chomont N, et al. Upregulation of PD-1 expression on HIV-specific CD8+ T cells leads to reversible immune dysfunction. Nat Med **2006**; 12:1198–202.
16. D'Souza M, Fontenot AP, Mack DG, et al. Programmed death 1 expression on HIV-specific CD4+ T cells is driven by viral replication and associated with T cell dysfunction. J Immunol **2007**; 179:1979–87.
17. Hafler DA, Kuchroo V. TIMs: central regulators of immune responses. J Exp Med **2008**; 205:2699–701.
18. Zhu C, Anderson AC, Schubart A, et al. The Tim-3 ligand galectin-9 negatively regulates T helper type 1 immunity. Nat Immunol **2005**; 6:1245–52.
19. Jones RB, Ndhlovu LC, Barbour JD, et al. Tim-3 expression defines a novel population of dysfunctional T cells with highly elevated frequencies in progressive HIV-1 infection. J Exp Med **2008**; 205:2763–79.
20. Golden-Mason L, Palmer BE, Kassam N, et al. Negative immune regulator Tim-3 is overexpressed on T cells in hepatitis C virus infection and its blockade rescues dysfunctional CD4+ and CD8+ T cells. J Virol **2009**; 83:9122–30.
21. Koguchi K, Anderson DE, Yang L, O'Connor KC, Kuchroo VK, Hafler DA. Dysregulated T cell expression of TIM3 in multiple sclerosis. J Exp Med **2006**; 203:1413–8.
22. Vine AM, Witkover AD, Lloyd AL, et al. Polygenic control of human T lymphotropic virus type I (HTLV-I) provirus load and the risk of HTLV-I–associated myelopathy/tropical spastic paraparesis. J Infect Dis **2002**; 186:932–9.
23. Kubota R, Kawanishi T, Matsubara H, Manns A, Jacobson S. Demonstration of human T lymphotropic virus type I (HTLV-I) tax-specific CD8+ lymphocytes directly in peripheral blood of HTLV-I-associated myelopathy/tropical spastic paraparesis patients by intracellular cytokine detection. J Immunol **1998**; 161:482–8.
24. Sabouri AH, Usuku K, Hayashi D, et al. Impaired function of human T-lymphotropic virus type 1 (HTLV-1)–specific CD8+ T cells in HTLV-1-associated neurologic disease. Blood **2008**; 112:2411–20.
25. Yashiki S, Fujiyoshi T, Arima N, et al. HLA-A*26, HLA-B*4002, HLA-B*4006, and HLA-B*4801 alleles predispose to adult T cell leukemia: the limited recognition of HTLV type 1 tax peptide anchor motifs and epitopes to generate anti-HTLV type 1 tax CD8(+) cytotoxic T lymphocytes. AIDS Res Hum Retroviruses **2001**; 17:1047–61.
26. Kozako T, Arima N, Toji S, et al. Reduced frequency, diversity, and function of human T cell leukemia virus type 1–specific CD8+ T cell in adult T cell leukemia patients. J Immunol **2006**; 177:5718–26.
27. Bunce M, O'Neill CM, Barnardo MC, et al. Phototyping: comprehensive DNA typing for HLA-A, B, C, DRB1, DRB3, DRB4, DRB5 &

DQB1 by PCR with 144 primer mixes utilizing sequence-specific primers (PCR-SSP). Tissue Antigens **1995**; 46:355–67.
28. Betts MR, Brenchley JM, Price DA, et al. Sensitive and viable identification of antigen-specific CD8+ T cells by a flow cytometric assay for degranulation. J Immunol Methods **2003**; 281:65–78.
29. Lee B, Tanaka Y, Tozawa H. Monoclonal antibody defining tax protein of human T-cell leukemia virus type-I. Tohoku J Exp Med **1989**; 157:1–11.
30. Hanon E, Hall S, Taylor GP, et al. Abundant tax protein expression in CD4+ T cells infected with human T-cell lymphotropic virus type I (HTLV-I) is prevented by cytotoxic T lymphocytes. Blood **2000**; 95:1386–92.
31. Kozako T, Yoshimitsu M, Fujiwara H, et al. PD-1/PD-L1 expression in human T-cell leukemia virus type 1 carriers and adult T-cell leukemia/lymphoma patients. Leukemia **2009**; 23: 375–82.
32. Petrovas C, Price DA, Mattapallil J, et al. SIV-specific CD8+ T cells express high levels of PD1 and cytokines but have impaired proliferative capacity in acute and chronic SIVmac251 infection. Blood **2007**; 110:928–36.
33. Kasagi S, Kawano S, Okazaki T, et al. Anti-programmed cell death 1 antibody reduces CD4+PD-1+ T cells and relieves the lupus-like nephritis of NZB/W F1 mice. J Immunol **2010**; 184:2337–47.
34. Hokey DA, Johnson FB, Smith J, et al. Activation drives PD-1 expression during vaccine-specific proliferation and following lentiviral infection in macaques. Eur J Immunol **2008**; 38:1435–45.
35. Petrovas C, Casazza JP, Brenchley JM, et al. PD-1 is a regulator of virus-specific CD8+ T cell survival in HIV infection. J Exp Med **2006**; 203:2281–92.
36. Sieburg M, Tripp A, Ma JW, Feuer G. Human T-cell leukemia virus type 1 (HTLV-1) and HTLV-2 tax oncoproteins modulate cell cycle progression and apoptosis. J Virol **2004**; 78:10399–409.

OPEN ACCESS Freely available online

PLoS one

A Comprehensive Peptidome Profiling Technology for the Identification of Early Detection Biomarkers for Lung Adenocarcinoma

Koji Ueda[1]*, Naomi Saichi[1], Sachiko Takami[2], Daechun Kang[1,3], Atsuhiko Toyama[1,3,4], Yataro Daigo[3], Nobuhisa Ishikawa[5], Nobuoki Kohno[5], Kenji Tamura[6], Taro Shuin[6], Masato Nakayama[7], Taka-Aki Sato[4], Yusuke Nakamura[3], Hidewaki Nakagawa[1]*

1 Laboratory for Biomarker Development, Center for Genomic Medicine, RIKEN, Yokohama, Japan, **2** CSK Institute for Sustainability, Ltd., Tokyo, Japan, **3** Laboratory of Molecular Medicine, Human Genome Center, Institute of Medical Science, The University of Tokyo, Tokyo, Japan, **4** Shimadzu Corporation, Kyoto, Japan, **5** Department of Molecular and Internal Medicine, Hiroshima University, Hiroshima, Japan, **6** Department of Urology, Kochi University School of Medicine, Nankoku, Japan, **7** Toppan Printing Co., Ltd., Tokyo, Japan

Abstract

The mass spectrometry-based peptidomics approaches have proven its usefulness in several areas such as the discovery of physiologically active peptides or biomarker candidates derived from various biological fluids including blood and cerebrospinal fluid. However, to identify biomarkers that are reproducible and clinically applicable, development of a novel technology, which enables rapid, sensitive, and quantitative analysis using hundreds of clinical specimens, has been eagerly awaited. Here we report an integrative peptidomic approach for identification of lung cancer-specific serum peptide biomarkers. It is based on the one-step effective enrichment of peptidome fractions (molecular weight of 1,000–5,000) with size exclusion chromatography in combination with the precise label-free quantification analysis of nano-LC/MS/MS data set using Expressionist proteome server platform. We applied this method to 92 serum samples well-managed with our SOP (standard operating procedure) (30 healthy controls and 62 lung adenocarcinoma patients), and quantitatively assessed the detected 3,537 peptide signals. Among them, 118 peptides showed significantly altered serum levels between the control and lung cancer groups ($p<0.01$ and fold change >5.0). Subsequently we identified peptide sequences by MS/MS analysis and further assessed the reproducibility of Expressionist-based quantification results and their diagnostic powers by MRM-based relative-quantification analysis for 96 independently prepared serum samples and found that APOA4 273–283, FIBA 5–16, and LBN 306–313 should be clinically useful biomarkers for both early detection and tumor staging of lung cancer. Our peptidome profiling technology can provide simple, high-throughput, and reliable quantification of a large number of clinical samples, which is applicable for diverse peptidome-targeting biomarker discoveries using any types of biological specimens.

Citation: Ueda K, Saichi N, Takami S, Kang D, Toyama A, et al. (2011) A Comprehensive Peptidome Profiling Technology for the Identification of Early Detection Biomarkers for Lung Adenocarcinoma. PLoS ONE 6(4): e18567. doi:10.1371/journal.pone.0018567

Editor: Richard C. Willson, University of Houston, United States of America

Received November 16, 2010; **Accepted** March 4, 2011; **Published** April 12, 2011

Funding: This study was supported by Japanese Ministry of Education, Culture, Sports, Science and Technology (Wakate-A, 22680064, http://kaken.nii.ac.jp/ja/p/22680064). This study was also funded by Shimadzu Corporation, CSK Institute for Sustainability, Ltd., Toppan Printing Co., Ltd. As employers of ST, AT, TS, or MN in this study, these funders did play a role in the study design, data collection and analysis, decision to publish, or preparation of the manuscript.

Competing Interests: ST is an employee of CSK Institute for Sustainability, Ltd. AT and TS are employees of Shimadzu Corporation. MN is an employee of Toppan Printing Co., Ltd. They contributed to the technical support and data analysis of this manuscript. The companies listed above also funded for this study, since this collaborative work was performed in "the academic-industrial alliance project for the development of lung cancer early detection system" among RIKEN, the University of Tokyo, Shimadzu Corporation, Toppan Printing Co., Ltd., and CSK Institute for Sustainability, Ltd. This does not alter the authors' adherence to all the PLoS ONE policies on sharing data and materials.

* E-mail: k-ueda@riken.jp (KU); hidewaki@ims.u-tokyo.ac.jp (HN)

Introduction

Lung cancer is the leading cause of cancer death worldwide [1]. Smoking is still the leading risk factor for lung cancer, but recently the proportion of never smoker-related lung cancer is significantly increasing, although its cause or other risk factor(s) is unknown [2]. Lung cancer patients show the poor prognosis with an overall 5-year survival rate of only 15% [3]. One of the reasons for this dismal prognosis is no effective tools to detect it at an early stage and in fact only 16% of patients are diagnosed at their early stage of the disease [3]. Current screening methods such as chest X-ray or cytological examination of sputum have not yet shown their effectiveness in the improvement of mortality of lung cancer, whereas low dose helical CT have been proved to possess a potential to detect early-stage lung cancer and demonstrate 20% lower lung cancer mortality rate compared to chest X-ray screening [4]. On the other hand, serum biomarkers for lung cancer have been investigated to achieve early detection of the disease and improve clinical management of patients [5]. Nonetheless, their present clinical usefulness remains limited [6,7]. CEA (carcinoembryonic antigen) and CYFRA (cytokeratin 19 fragment) are elevated in sera in a subset of lung cancer patients, and are clinically applied to monitor the disease status and evaluate the response to treatments. However, they are not recommended to use in clinical diagnosis and screening [8] because they are also elevated in certain non-cancerous conditions

such as smoking and lung inflammation as well as in patients with other types of cancers. It is obvious that CEA and CYFRA do not have the sufficient power to apply for the screening of early-stage lung cancer. Hence, development of novel serum/plasma biomarkers applicable for lung cancer diagnosis is urgently required.

Recently monitoring the protein expression pattern in clinical specimens by proteomics technologies has offered great opportunities to discover potentially new biomarkers for cancer diagnosis. Various proteomic tools such as 2D-DIGE, SELDI-TOF-MS, protein arrays, ICAT, iTRAQ and MudPIT have been used for differential analysis of biological samples including cell lysates and blood to better understand the molecular basis of cancer pathogenesis and the characterization of disease-associated proteins [9]. In order to explore putative biomarkers in complicated biological samples, focused proteomics or targeted proteomics technologies have been utilized such as; phosphoprotein enrichment technologies IMAC [10], the cell-surface-capturing (CSC) technology [11,12], glycan structure-specific quantification technology IGEL [13]. Most recently, to identify novel lung cancer biomarkers, Ostroff *et al.* reported the aptamer-based proteomic technology targeting 813 known proteins. Finally they selected 12 proteins which discriminated NSCLC from controls with 89% sensitivity and 83% specificity [14]. Thus targeted proteomics technologies such as the aptamer method would be applicable for the measurement of already known proteins, however could not be applied for the discovery of biomarkers targeting unknown proteins, post translational modifications, or biologically-processed polypeptides.

These methods can circumvent the technological limitations that currently prohibit the sensitive and high-throughput profiling of, in particular, blood proteome samples because of its high complexity and large dynamic range of proteins. The peptidome profiling technology addressed in the present study is one of the focused proteomics approaches targeting on biosynthetic fragments of proteins/peptides in blood, involving bioactive peptides and those non-specifically degraded by proteases or peptidases [15,16].

So far more than 500 proteases/peptidases are known to be expressed in human cells [17,18]. They function at almost all locations in the body including intracellular region, extracellular matrices, and in blood, involved in activation of other protein functions, degradation of cellular proteins, and notably tumor progression or suppression [19,20,21]. Indeed many matrix metalloproteases are overexpressed in various types of tumor cells, that facilitate construction of favorable micro-environment for tumor cells or promotion of metastasis[21]. Definitely these protease/peptidase activities should result in the production of digested peptide fragments well reflecting the tumor progression or tumor-associated responses. Thus peptidomic profiling of human serum or plasma is a promising tool for the discovery of novel tumor markers.

In this article, we extracted peptidome fractions (molecular weight <5,000 Da) from 92 individuals using the well-established and reproducible one-step peptidome enrichment method based on size exclusion chromatography (SEC) [22,23] and provided them to the label-free mass spectrometric quantification analysis combined with the statistical analyses on Expressionist proteome server platform. Our rapid and simple peptidome enrichment procedure can circumvent both less reproducible peptidome extraction by such as ultrafiltration spin filters and prolonged sample preparation including immuno-depletion column chromatography, denaturing proteins, buffer exchange, ultrafiltration, and so on [16]. After quantitative comparison of 3,537 serum peptides among 92 cases in the lung cancer biomarker discovery, we further evaluated the accuracy of quantification results by another more reliable quantification method MRM (multiple reaction monitoring) technology using independently prepared 96 serum samples.

Materials and Methods

Serum samples

All human serum samples were obtained with informed consent from 122 patients with lung adenocarcinoma (stage I to IV) at Hiroshima University Hospital at the examination on admission. Serum samples as normal controls were also obtained with informed consent from 30 healthy volunteers who received medical checkup at Hiroshima NTT Hospital and 36 from Kochi University Hospital. Each consent above was given in writing. To circumvent undesirable degradation of proteins and peptides, all serum samples were collected and stored under unified SOP. Briefly, all venous blood specimens were collected with vacuum blood collection tubes TERUMO VP-P070K (TERUMO, Tokyo, Japan). After staying upright at ambient temperature for 60 minutes, serum fractions were separated with centrifugation at 1500 x *g* for 15 min (4°C) and immediately stored at −80 °C. One freeze-and-thaw procedure was permitted for any serum samples used in the present study. This study was approved by individual institutional ethical committees; The Ethical Committee of Yokohama Institute, RIKEN (Approval code: Yokohama H20-12), The Ethical Committee of Hiroshima University Hospital, and The Ethical Committee of Kochi University Hospital.

Heat inactivation of sera and subsequent peptidome enrichment

All serum samples were freezed and thawed once and immediately incubated at 100 °C for 10 minutes after 4 times dilution with proteomics grade water. Following filtration with Spin-X 0.45 μm spin filters (Corning Incorporated, Corning, NY, USA), samples were loaded into 10/300 Superdex peptide column (GE Healthcare UK Ltd., Buckinghamshire, England) coupled with Prominence HPLC system (Shimadzu Corporation, Kyoto, Japan). The peptidome fraction was collected from 22 to 34 minutes in the constant flow of 100 mM ammonium acetate at 0.5 ml/min flow rate. The collected fractions were dried-up with Vacuum Spin Drier (TAITEC Co., Ltd., Saitama, Japan).

LC/MS/MS analysis for the screening study

The dried peptide samples were resuspended in 2% acetonitrile with 0.1% trifluoroacetic acid and analyzed by QSTAR-Elite mass spectrometer (AB Sciex, Foster City, CA, USA) combined with UltiMate 3000 nano-flow HPLC system (DIONEX Corporation, Sunnyvale, CA, USA). Samples were separated on the 100 μm×200 mm tip-column (GL Sciences Inc., Tokyo, Japan), in which L-Column beads (Chemicals Evaluation and Research Institute, Tokyo, Japan) were manually loaded, using solvent A [0.1% formic acid, 2% acetonitrile] and solvent B [0.1% formic acid, 70% acetonitrile] with the multistep linear gradient of solvent B 5 to 55% for 95 minutes and 55 to 95% for 10 minutes at a flow rate 200 nl/min. The elute was directly analyzed with the 1 second MS survey (m/z 400–1800) followed by three MS/MS measurements on the most intense parent ions (30 counts threshold, +2 - +4 charge state, and m/z range 50–2000), using the "smart exit" setting (SIDA = 3.0, max accumulation time = 2.0 sec.). Previously targeted parent ions were excluded from repetitive MS/MS acquisition for 40 seconds (100 mDa mass tolerance). The other parameters on QSTAR-Elite were shown as follows: DP = 60, FP = 265, DP2 = 15, CAD = 5, IRD = 6,

IRW = 5, Curtain gas = 20, and Ion spray voltage = 1600 V. The mass of each run was calibrated using three typical polysiloxane-derived background peaks: m/z = 445.12003, 519.13882, and 667.17640. The resolution of mass spectra was around 20,000 at m/z = 400. The primary data files (formatted as wiff and wiff.scan) from 92 clinical samples are available in a public repository site Proteome Commons (https://proteomecommons.org/). The MASCOT database search was performed on the Analyst QS 2.0 software (AB Sciex, Foster City, CA, USA). The MS/MS data was searched against the human protein database from SwissProt 57.4 (20,400 sequences) using the search parameters: Taxonomy = Homo sapiense, Enzyme = None, Fixed modifications = None, Variable modifications = Oxidation (Met), MS tolerance = 50 ppm, and MS/MS tolerance = 0.1 Da, with Mascot Automatic Decoy Search. Although Matrix Science recommends to use the Homology threshold for less-stringent criteria or Identity threshold providing almost same protein identification numbers with the criteria Expectation value <0.05 (http://www.matrixscience.com/help/interpretation_help.html), we accepted peptide identifications that satisfied both the false discovery rate (FDR) of peptide matches above identity threshold less than 5% and the Expectation value <0.05 in order to obtain more reliable identification of individual peptides than that from Mascot default criteria.

Alignment of MS chromatogram planes and peak detection on Expressionist RefinerMS

The raw data files from QSTAR-Elite (.wiff and wiff.scan formatted) were directly loaded onto the Genedata Expressionist modules (Genedata AG, Basel, Switzerland). Genedata Expressionist worked on the in-house server system HP-DL380-G5 (Hewlett-Packard Development Company, Palo Alto, CA, USA) equipped with 16 GB memory, (72 GB×2) + (146 GB×25) RAID 0+1 hard disks, and SUSE Linux Enterprise Server 10 SP2 operating system, installed with Oracle 10 g ver. 10.2.0.4. software (Oracle Corporation, Redwood Shores, CA, USA). All MS chromatograms were smoothed with RT Window = 3 scans in the Chromatogram Chemical Noise Subtraction Activity. To remove the background noise, a peak intensity is defined as follows.

$$\text{Intensity}_{\text{subtracted}} = \max(\text{Intensity}_{\text{original}} - \text{Quantile} - \text{Threshold}, 0)$$

Here, values Quantile = 50%, Intensity Threshold = 15 cps were used. Furthermore signals satisfying at least one of the following criteria were considered as noise peaks and subtracted: RT Window >50 scans, Minimum RT Length = 4 scans, or Minimum m/z Length = 8 data points. Then MS chromatogram planes derived from 92 serum samples were accurately aligned using parameters: m/z Window = 0.1 Da, RT Window = 0.2 min, Gap Penalty = 1, and RT Search Interval = 5 min in the Chromatogram RT Alignment Activity. Next, the Summed Peak Detection Activity detected the peaks on a temporary averaged chromatogram with parameters as follows: Summation Window = 5 scans, Overlap = 50, Minimum Peak Size = 4 scans, Maximum Merge Distance = 10 data points, Gap/Peak Ratio = 1, Method = curvature-based peak detection, Peak Refinement Threshold = 5, Consistency Filter Threshold = 0.8, Signal/Noise Threshold = 1. Finally the two steps Summed Isotope Clustering Activity identified isotope patterns among 2D peaks, in which peaks identified as belonging to the same isotope pattern of a molecule were grouped into peak clusters. The first clustering was performed with the following criteria: Minimum Charge = 1, Maximum Charge = 10, Maximum Missing Peaks = 0, First Allowed Gap Position = 3, Ionization = protonation, RT Tolerance = 0.1 min, m/z Tolerance = 0.05 Da, Isotope Shape Tolerance = 10.0, and Minimum Cluster Size Ratio = 1.2. The second clustering was performed with the same setting above, except for Minimum Cluster Size Ratio = 0.6 and Reuse Existing Clusters = true. The information of all detected cluster peaks, including m/z, retention time, and intensity, was exported as ABS files.

Label-free quantification and statistical analysis on Expressionist Analyst

The ABS files were loaded on the Expressionist Analyst module (Genedata AG, Basel, Switzerland). The peak intensity variation among 32 samples was normalized by fixing the median intensity of each sample at 10,000. Using the normalized intensity data, Student's t-test was performed between the normal group (n = 30) and lung cancer patients group (n = 62). The candidate biomarker peaks were extracted which showed $p<0.01$ and fold-change >5.0 between two groups. The candidates were further selected by Absent/Present Search to identify peaks with all-or-nothing detection pattern, which were detectable in 15 or all of 16 samples in one group and 1 or none of 16 samples in another group.

Multiple Reaction Monitoring

Serum samples were processed with Superdex peptide column chromatography as described above before mass spectrometric analyses. The dried peptide samples were resuspended with 1 fmol/μl BSA tryptic digest solution in 2% acetonitrile, 0.1% trifluoroacetic acid and analyzed by 4000 QTRAP mass spectrometer (AB Sciex, Foster City, CA, USA) combined with Paradigm MS4 PAL nano-flow HPLC system (AMR Inc., Tokyo, Japan). Peptides were separated on the 100 μm×100 mm tip-column (GL Sciences Inc., Tokyo, Japan), in which L-Column ODS beads (Chemicals Evaluation and Research Institute, Saitama, Japan) were manually loaded. Using solvent A [0.1% formic acid, 2% acetonitrile] and solvent B [0.1% formic acid, 90% acetonitrile], the linear gradient of solvent B 2 to 100% for 10 minutes was configured at a flow rate 200 nl/min. 19 targeted peptide ions and 5 BSA-derived peptide ions were simultaneously monitored by the MRM mode in Analyst 1.5 software (AB Sciex, Foster City, CA, USA) in duplicate. The MRM transitions are shown in **Table S4**. The acquired MRM chromatograms were then smoothened and quantified with MultiQuant software (AB Sciex, Foster City, CA, USA). MRM peak areas in each sample were normalized as follows:

$$\text{Area}_{\text{Normalized}} = \text{Area}_{\text{Raw data}}/(\text{summed area of 5 BSA standards}) \times 1000$$

Box plot analysis and ROC curve analysis

The averaged area of the duplicated MRM chromatogram peak corresponding to 19 candidate biomarker peptides was used to create box plot with R algorithm. For each study the box represents the middle half of the distribution of the data points stretching from the 25th percentile to the 75th percentile. The line across the box represents the median. The lengths of the lines above and below the box are defined by the maximum and minimum datapoint values, respectively, that lie within 1.5 times the spread of the box. Results of Student's t-test were included on the box plot. ROC curves were also depicted by R. The cut-off value was set at the point whose

distance from the (sensitivity, specificity) = (1, 1) reached the minimum. The sensitivity (Sens), specificity (Spec), positive predictive value (PV+), negative predictive value (PV-), and are under the curve (AUC) were shown on each graph.

Results

The efficient enrichment of peptidome fractions from sera

Since reproducible and accurate separation of the peptidome fraction from serum was essential for the effective screening of biomarkers, we optimized a simple gel filtration chromatography method (Fig. 1) and evaluated the peptide recovery. To avoid uncontrolled degradation of serum components arising from intact proteases and peptidases, all serum samples were immediately heated at 100 °C for 10 min after only one freeze-thaw procedure. Four-fold dilution of serum with water could eliminate the protein aggregation during heat inactivation even though the samples appeared slightly cloudy. Figure 2*A* shows the merged gel filtration HPLC chromatograms from 16 individual serum samples using the Superdex Peptide 10/300 column. The spectra illustrated highly reproducible separation of serum proteins and peptides. Then, the accuracy of size exclusion chromatography was assessed by analyzing 10 fractions (2 min each from retention time for the period of 14–34 min, Fig. 2*B*) with the MALDI-TOF-TOF mass spectrometer (Fig. 2*C*). As shown by the continuous MS spectra in Figure 2*C*, our gel filtration chromatography procedure allowed precise separation of serum proteins and peptides based on their molecular weights. Consequently we defined the fraction numbers 5 to 10 (corresponding to molecular weight 1,000 to 5,000) that should be focused in the further biomarker screening and validation studies.

Label-free quantification-based peptide biomarker screening for lung cancer

To explore serum peptides which could be applied for early detection of lung cancer, we acquired quantitative peptidome

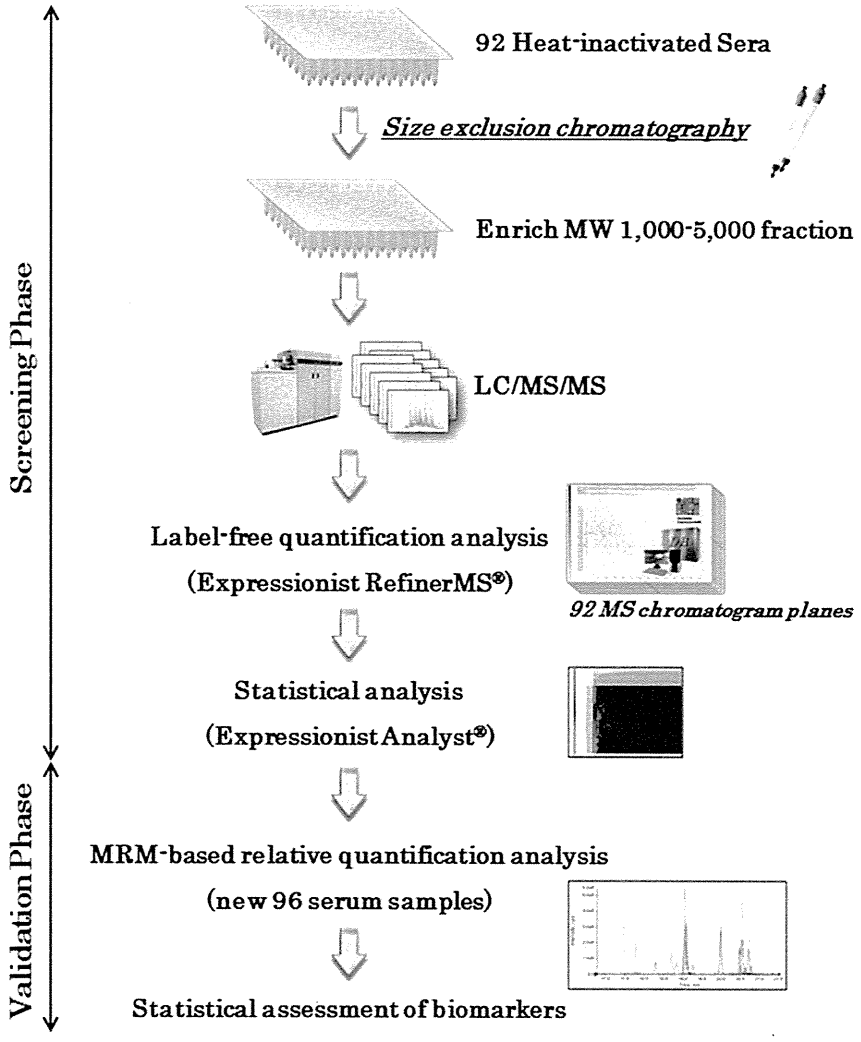

Figure 1. Schematic view of peptidome biomarker development workflow. In the screening phase, 92 serum samples were initially heat inactivated. The peptidome fractions enriched with gel filtration chromatography were analyzed with QSTAR-Elite LC/MS/MS. Following LC/MS data processing and label-free quantification analysis on the Expressionist RefinerMS module, candidate biomarkers were statistically extracted by the Expressionist Analyst module. In the validation phase, MRM experiments were performed to assess the applicability of 19 biomarker candidates using additional 96 serum samples.
doi:10.1371/journal.pone.0018567.g001

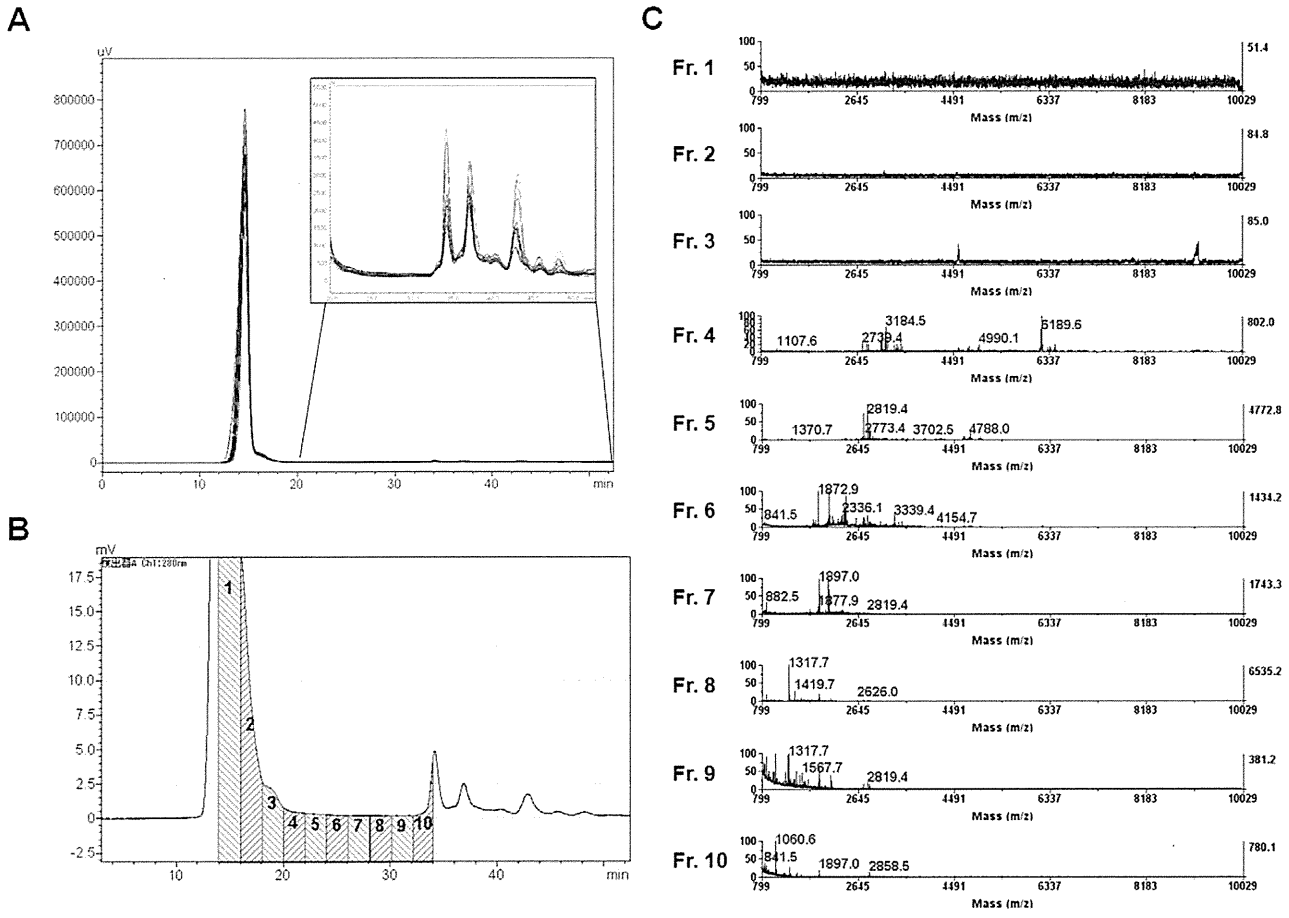

Figure 2. Simple and efficient enrichment of serum peptidome fractions by gel filtration chromatography. (*A*) The merged display of 16 independent spectra of gel filtration chromatography (280 nm UV absorbance). 10 µl each of serum sample was loaded. The upper right box shows the magnified view of the retention time range from 20 to 50 minutes. (*B*)(*C*) To evaluate the fractionation efficacy of Superdex Peptide 10/300 column, the elute was separated into 10 fractions and analyzed with MALDI-TOF mass spectrometer. The numbers of fractions in *B* correspond to the spectra numbers in *C*.
doi:10.1371/journal.pone.0018567.g002

profiles from 92 individuals (**Table S1**) including 62 lung cancer patients that consisted of 32 patients with an operable lung cancer (stage-I: n = 10, stage-II: n = 10, stage-IIIa: n = 12) and 30 lung cancer patients at an advanced stage (stage-IIIb: n = 15, stage-IV: n = 15) to identify candidate serum biomarkers for lung cancer. The serum samples were purified using gel filtration chromatography as described above and individually subjected to LC/MS/MS analyses using QSTAR-Elite mass spectrometer (Fig. 1). Subsequently 92 MS raw data were loaded and processed on the Expressionist RefinerMS module (Fig. 3*A*). Genedata Expressionist is an enterprise system for omics data management comprised of integrated software modules, which support the complete R&D processes involving data processing, statistical analysis, data management and result reporting. The technology-dependent modules for microarray data (Refiner Array), mass spectrometry (Refiner MS, used in the present study) and genomic profiling (Refiner Genome) allow highly-sophisticated data processing, quantification, visualization, and result exporting in any generally-used formats. Once all data are quantified and summarized, they can be seamlessly analyzed with the Genedata Analyst module employing various statistical analyses. This system initially made the MS chromatogram planes as shown in Figure 3*C*, and subtracted the instrument specific noises and chemical noises effectively. At the fourth step of the workflow in Figure 3*A*, the retention time (RT) grids on each MS chromatogram plane were perfectly aligned among these 92 samples (Fig. 3*B*), which allowed the solid quantification analysis of multiple samples. Subsequently, peaks were detected from temporarily averaged m/z-RT planes by the Chromatogram Summed Peak Detection Activity in order to avoid missing peak-location information even if the peaks were not detectable in particular planes. The detected isotopic peaks belonging to the same peptide signals were grouped into individual clusters that are displayed as colored rectangles in Figure 3*C*. A total of 12,396 non-redundant isotopic peak clusters with charge state +1 to +10 were detected from 92 serum samples. We then utilized 3,537 clusters with charge stage +2 to +10 for further statistical considerations in the Expressionist Analyst module, since singly-charged ions might include substantial proportion of non-peptide components such as chemicals.

Student's t-test was applied to investigate the differences in their serum levels between the normal group (n = 30) and the lung cancer group (n = 62) (Fig. 4*A*). This analysis identified 118 candidate biomarker peptides ($p<0.01$ and fold-change of >5.0). Since the criteria of t-test were variable for the purpose of candidate selection, we used the threshold above just in order to define the highest priority group. The intensity distributions of these peptides were

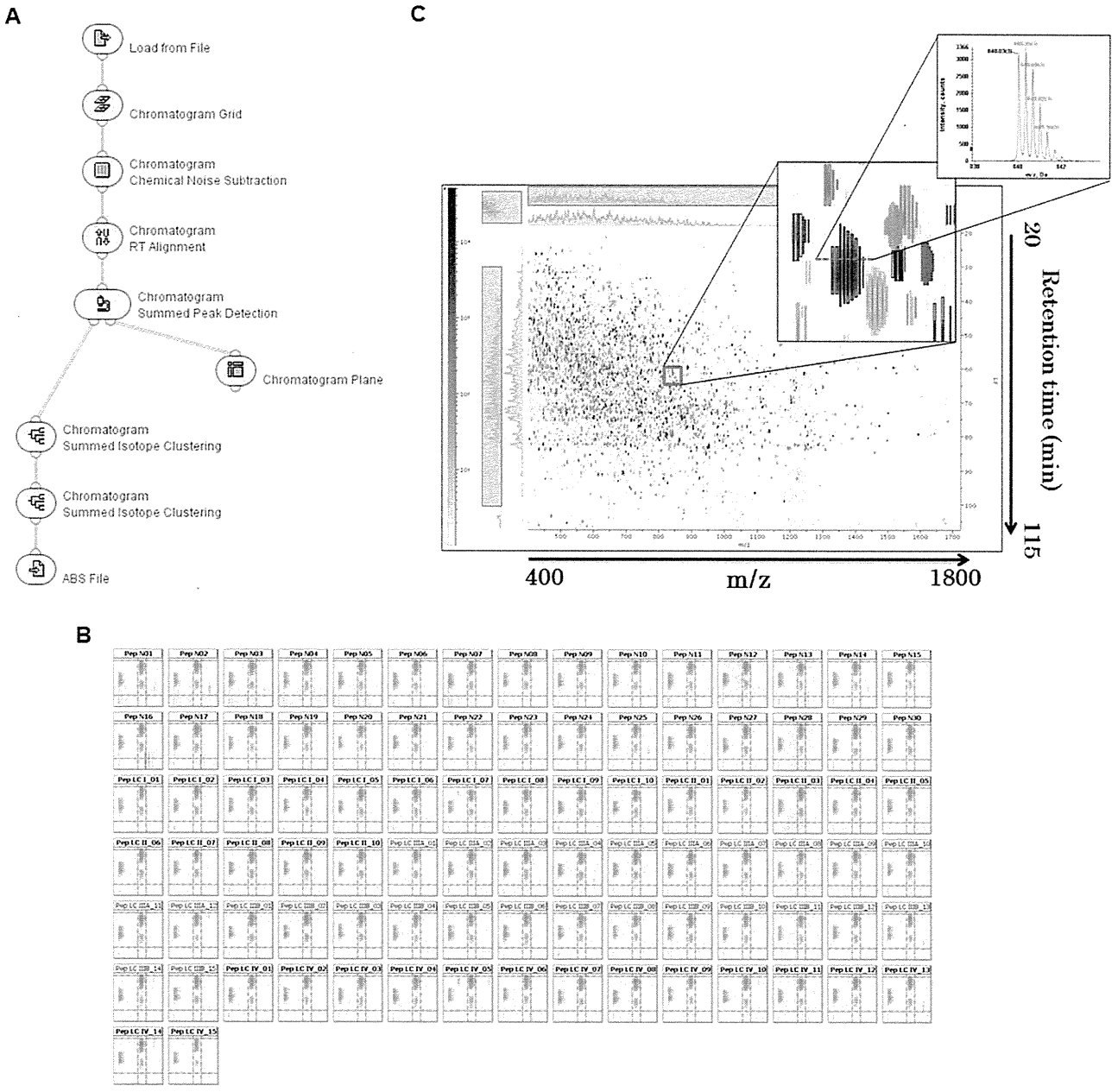

Figure 3. Rapid and accurate data processing for label-free quantification on the Expressionist RefinerMS module. (*A*) The total workflow used in the Expressionist RefinerMS module. Only 3 hours were needed to complete entire steps in this workflow on 92 LC/MS/MS data (each with 120 minutes LC gradient). (*B*) The representative area of m/z - retention time planes after RT alignment of 92 LC/MS/MS data. In each panel, three isotopic clusters and grid lines were displayed, showing highly exact alignments. (*C*) The MS chromatogram plane in which all data processing were completed. Finally, isotopic clusters derived from a single peptide were grouped into a colored cluster as shown in the middle panel. The far right panel shows the MS spectrum corresponding to the horizontal section view of a representative cluster.
doi:10.1371/journal.pone.0018567.g003

visualized with bar charts in Figure S1. The subsequent principal component analysis demonstrated that the values of 118 candidate biomarker peptides could explicitly separate control and lung cancer groups on the 3D plot using principal component 1, 2, and 3 (Fig. 4*B*). The proportion of variance described by the principal component 1, 2, or 3 was 66.9%, 15.0%, or 4.4%, respectively, indicating that illustrated components 1 to 3 could reflect 86.3% (the cumulative proportion) of quantitative information in this mass spectrometric screening analysis.

Identification of peptide sequences by LC/MS/MS

Alongside the label-free quantification-based biomarker screening described above, the comprehensive peptide sequencing was performed by a combination of QSTAR-Elite LC/MS/MS analysis and MASCOT database search. Among 230,657 MS/MS queries from 92 serum samples, 5,382 peptides were successfully sequenced with MASCOT expectation value <0.05 (FDR of peptide matches above Identity threshold was 1.49%). After examining redundancy, 424 unique peptides were

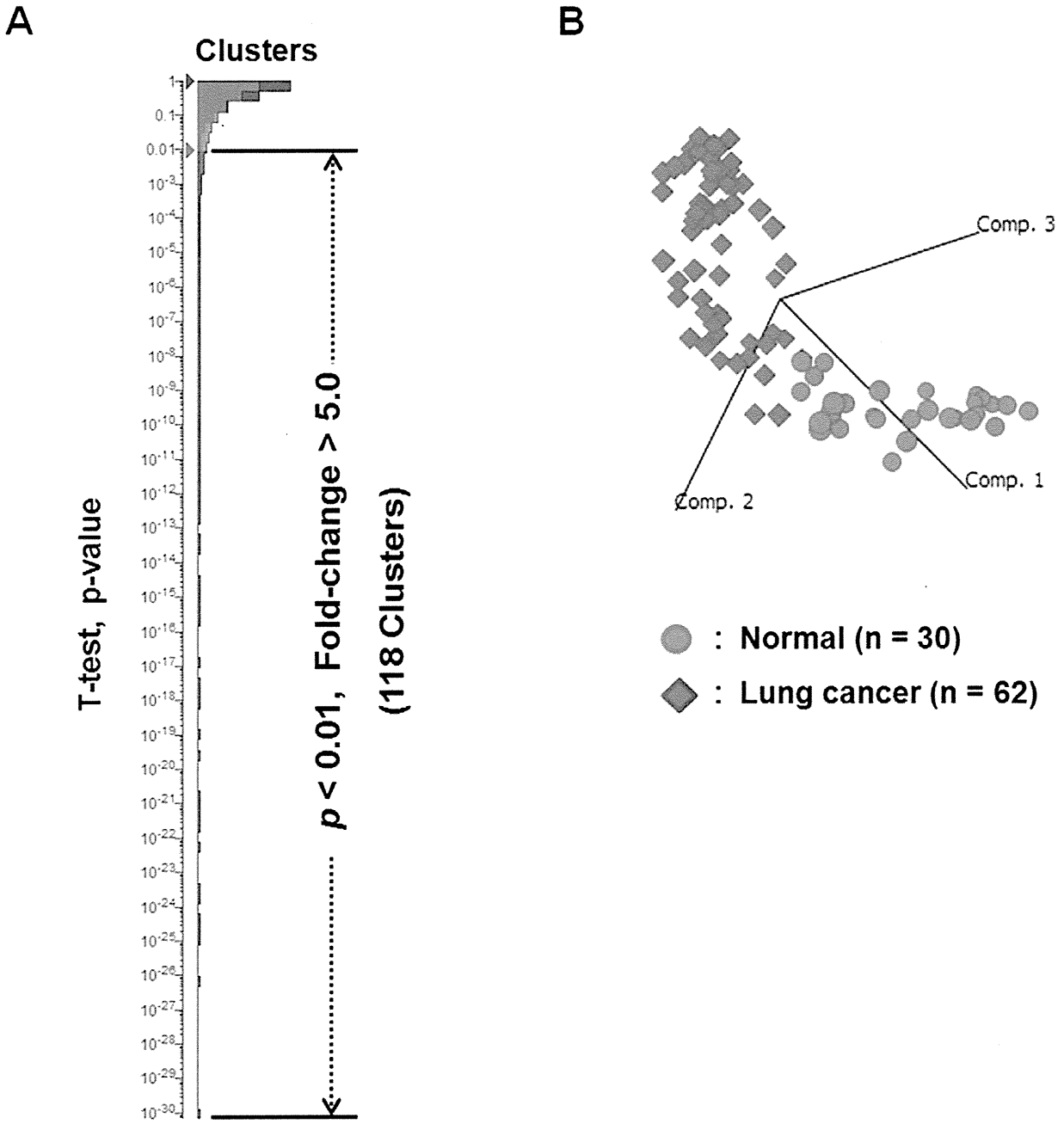

Figure 4. Statistical identification of candidate biomarkers for lung cancer. (*A*) The hierarchy chart of clusters (peptides) according to Student's t-test p-values (normal group vs. lung cancer group). 118 peptides satisfied the criteria of $p<0.01$ and fold change >5.0. (*B*) Principal component analysis using the values of 118 candidate biomarker peptides showed clear separation between control and lung cancer groups on the 3D plot. The proportion of variance described by the principal component 1, 2, or 3 was 66.9%, 15.0%, or 4.4%, respectively.
doi:10.1371/journal.pone.0018567.g004

identified that corresponded to 106 proteins (**Table S2**). Regarding the 118 candidate peptides, 19 peptides were uniquely identified; 12 of them were found to be derivatives from fibrinogen alpha chain (FIBA), 4 from apolipoprotein A-IV (APOA4), and the remaining three peptides were turned out to be a fragment of amiloride-sensitive cation channel 4 (ACCN4), apolipoprotein E (APOE), and limbin (LBN) (**Table 1**).

MRM-based validation experiment for 19 candidate biomarker peptides

To assess the quantitative reproducibility of the label-free quantification results in our single-run screening analysis, as well as the clinical usefulness of the 19 candidate biomarkers, we conducted further validation studies by multiple reaction monitoring (MRM) technology using 96 additional serum samples (**Table S1**). For designing the optimum MRM transitions specific

Table 1. 19 lung cancer biomarker candidates.

Expressionist [a]					MASCOT [b]			
Cluster ID [c]	m/z	RT	z	t-test p-value [d]	Acc. [e]	start	end	Peptide sequence
Cluster_3187	551.8	64.1	2	1.54E-15	ACCN4	613	624	CPSLGRAEGGGV
Cluster_3858	750.9	60.3	2	7.85E-04	APOA4	271	283	ELGGHLDQQVEEF
Cluster_3444	629.8	52.2	2	9.41E-07	APOA4	268	284	GGHLDQQVEEF
Cluster_3661	689.8	75.3	2	8.52E-08	APOA4	260	284	GNTEGLQKSLAELGGHLDQQVEEFR
Cluster_3498	643.3	65.7	2	6.08E-05	APOA4	288	304	SLAELGGHLDQQVEEFR
Cluster_2454	756.4	65.6	3	2.93E-03	APOE	194	214	TVGSLAGQPLQERAQAWGERL
Cluster_248	768.8	53.0	2	6.41E-23	FIBA	1	16	ADSGEGDFLAEGGGVR
Cluster_126	432.7	62.6	2	3.07E-22	FIBA	7	15	DFLAEGGGV
Cluster_159	510.7	49.9	2	5.75E-25	FIBA	7	16	DFLAEGGGVR
Cluster_240	733.3	56.5	2	3.80E-15	FIBA	2	16	DSGEGDFLAEGGGVR
Cluster_166	525.7	62.8	2	2.99E-25	FIBA	5	15	EGDFLAEGGGV
Cluster_3342	603.8	50.7	2	8.17E-27	FIBA	5	16	EGDFLAEGGGVR
Cluster_2872	461.2	61.8	2	3.31E-12	FIBA	6	15	GDFLAEGGGV
Cluster_174	539.3	52.3	2	4.10E-15	FIBA	6	16	GDFLAEGGGVR
Cluster_180	554.2	63.5	2	5.37E-22	FIBA	4	15	GEGDFLAEGGGV
Cluster_207	632.3	52.1	2	1.98E-21	FIBA	4	16	GEGDFLAEGGGVR
Cluster_196	597.8	63.2	2	4.44E-24	FIBA	3	15	SGEGDFLAEGGGV
Cluster_221	675.8	52.3	2	2.22E-22	FIBA	3	16	SGEGDFLAEGGGVR
Cluster_135	453.2	39.0	2	2.81E-24	LBN	306	313	FLLSLVLT

[a]Information acquired from the Expressionist RefinerMS or the Analyst module.
[b]Information acquired from MASCOT database search.
[c]Each ID corresponds to that in the bar chart (Fig. S1).
[d]Shown is the p-value of t-test between normal group and lung cancer group.
[e]UniProt Accession Number.
doi:10.1371/journal.pone.0018567.t001

to the 19 candidate peptides, the m/z values of precursor ions detected in the screening phase were set as Q1 channels and those of four most intense fragment ions were selected from each MS/MS spectrum for Q3 channels (Fig. S2 and Table S3). Hence, a total of 76 MRM transitions were simultaneously monitored by 4000 QTRAP mass spectrometry using a serum peptidome sample (Fig. 5). We then determined the specific eluting retention time for each candidate peptide and selected the optimum MRM transitions showing the highest MRM chromatogram peak out of four transitions for each peptide (Table S4). In our observations, only two peptides (FIBA 3–16 and FIBA 5–16) showed the identical orders of fragment ion intensities between QSTAR-Elite and 4000 QTRAP systems as shown in Figure 5. We further performed MRM-based relative quantification analysis using 36 normal controls and 60 lung cancer samples in duplicated experiments. The serum levels of 19 candidate biomarker peptides were calculated on the basis of normalized and averaged MRM chromatogram peak areas and displayed with box plots (Fig. 6*A*). To evaluate the efficacy of these candidates for early detection of lung cancer, we compared the earlier-stage lung cancer group (stage-I, II, and IIIa) with the normal group by Student's t-test. The results revealed that 15 out of 19 candidate peptides showed significant differences in their serum levels between the two groups, while 4 peptides (FIBA 4–15, FIBA 5–15, FIBA 7–15, and FIBA 7–16) showed no significant differences. Concerning the comparison between the normal group and the advanced-stage lung cancer group (stage-IIIb and IV), similarly 4 peptides (APOA4 268–284, APOA4 271–283, FIBA 5–15, and APOE 194–214) did not satisfy the criterion of $p<0.05$. Hence, we considered that the remaining 12 peptides are likely to be more promising biomarkers for lung cancer diagnosis. We next assessed the sensitivity and specificity of the 19 biomarkers for lung cancer diagnosis by ROC curve analysis (Fig. 6*B* and Fig. S3). The cut-off value was set at the point whose distance from the (sensitivity, specificity) = (1, 1) reached the minimum. Given the value of sensitivity to detect lung cancer at an earlier stage, FIBA 6–15 (87.1%), APOA4 273–283 (61.3%), FIBA 5–16 (58.1%), and LBN 306–313 (58.1%) appeared to be the good biomarker candidates. However although the specificity of APOA4 273–283, FIBA 5–16, and LBN 306–313 were remarkably higher (88.9%, 94.4%, and 100%, respectively, Fig. 6*B*), FIBA 6–15 showed relatively lower specificity (44.4%) and the area under the curve (0.641). By integrating the results from t-test and ROC curve analysis, the 3 candidates shown in Figure 6*B* were considered as the most promising peptide biomarkers for early detection of lung cancer.

Discussion

Even though recent mass spectrometry instruments have allowed measurements of peptide mixtures at high sensitivity [24], enrichment of targeted proteins/peptides is still indispensable to achieving detection and identification of serum components in limited amounts of biological materials. In this sense, the methodology to purify preanalytical samples without loss of targeted components is crucial. From this point of view, the previous peptidome profiling technologies, such as SELDI-TOF-MS coupled with ProteinChip arrays or MALDI-TOF-MS

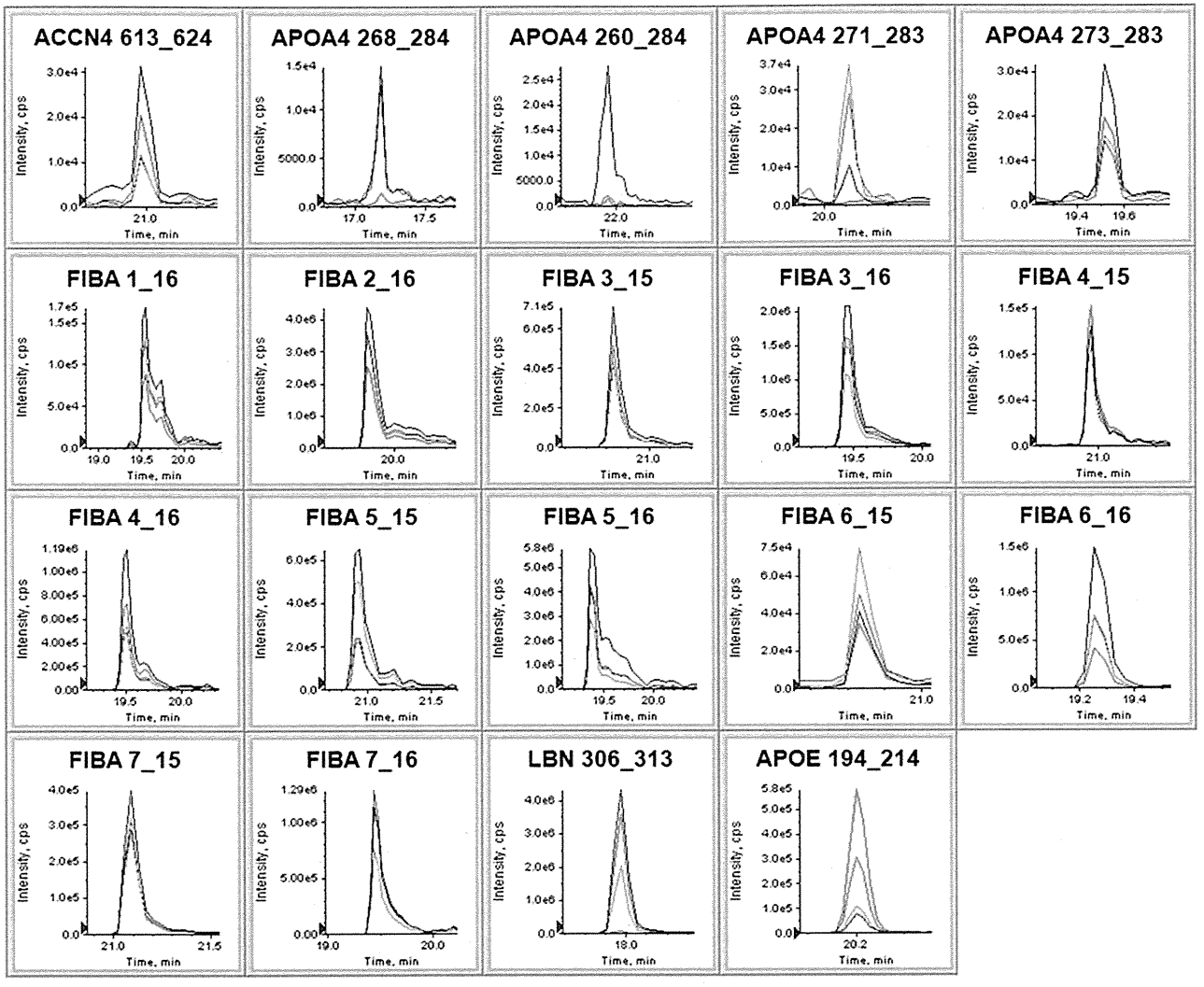

Figure 5. Selection and confirmation of the optimum MRM transitions for 19 candidates. Four pairs of precursor m/z and fragment m/z (Q1/Q3 channels) were set as MRM transitions for each peptide. The blue, red, green, or gray MRM chromatogram monitored the fragment ion which showed the 1st, 2nd, 3rd, or 4th most intense peaks in QSTAR-Elite LC/MS/MS analysis, respectively.
doi:10.1371/journal.pone.0018567.g005

analysis of ClinProt magnetic beads-purified samples, covered only limited spectra of serum peptidome. Most of studies utilizing ion-exchange selection or reversed phase extraction of peptidome on ProteinChip arrays [25,26,27] or magnetic beads [28,29] allowed at most 200 peak detections within the mass range 1,000 to 20,000. Meanwhile our peptidome profiling technology consisting of gel-filtration chromatography, custom-made high resolution C18 tip-column, QSTAR-Elite mass spectrometer, and Expressionist proteome server platform analysis enabled us to detect 12,396 non-redundant molecules with charge state of +1 to +10. The number of detected peaks here denoted the enormous advantage of our methodology for the analytical comprehensiveness compared to other existing methods. Although we focused on serum peptides involved in 3,537 clusters with charge stage of +2 to +6 in this study, 12,396 clusters might include non-peptide serum components such as metabolites, which should be also valuable for biomarker screening. Additionally, regarding the capacity of sample numbers to be analyzed simultaneously, the Expressionist server platform has a potential to handle a larger number of clinical samples. Because we in fact needed only less than an hour to process 92 LC/MS/MS data in the Refiner MS module (Fig. 1*A*), a comprehensive analysis of up to 1,000 cases would be feasible in a day. Hence our peptidome profiling technology provides the outstanding features of data comprehensiveness and quantitative performance, which absolutely fit the in-depth screening of novel biomarkers from clinical samples such as serum and plasma compared to previous technologies described above, whereas estimating actual dynamic range of detected peptide concentrations would be needed by,for instance, MRM-based absolute quantification analysis in the future. It could be tailored to many diagnostic and pharmaco-dynamic purposes as comprehensive interpretations of catalytic and metabolic activities in body fluids or tissues.

By using this technology, we finally identified 19 serum peptides as candidate lung cancer biomarkers (Table 1). The subsequent MRM-based validation experiments and t-test resulted in the confirmation of 12 candidates as reliable lung cancer biomarkers (Fig. 6*A*). Eight of them were fragments derived from fibrinopep-

A

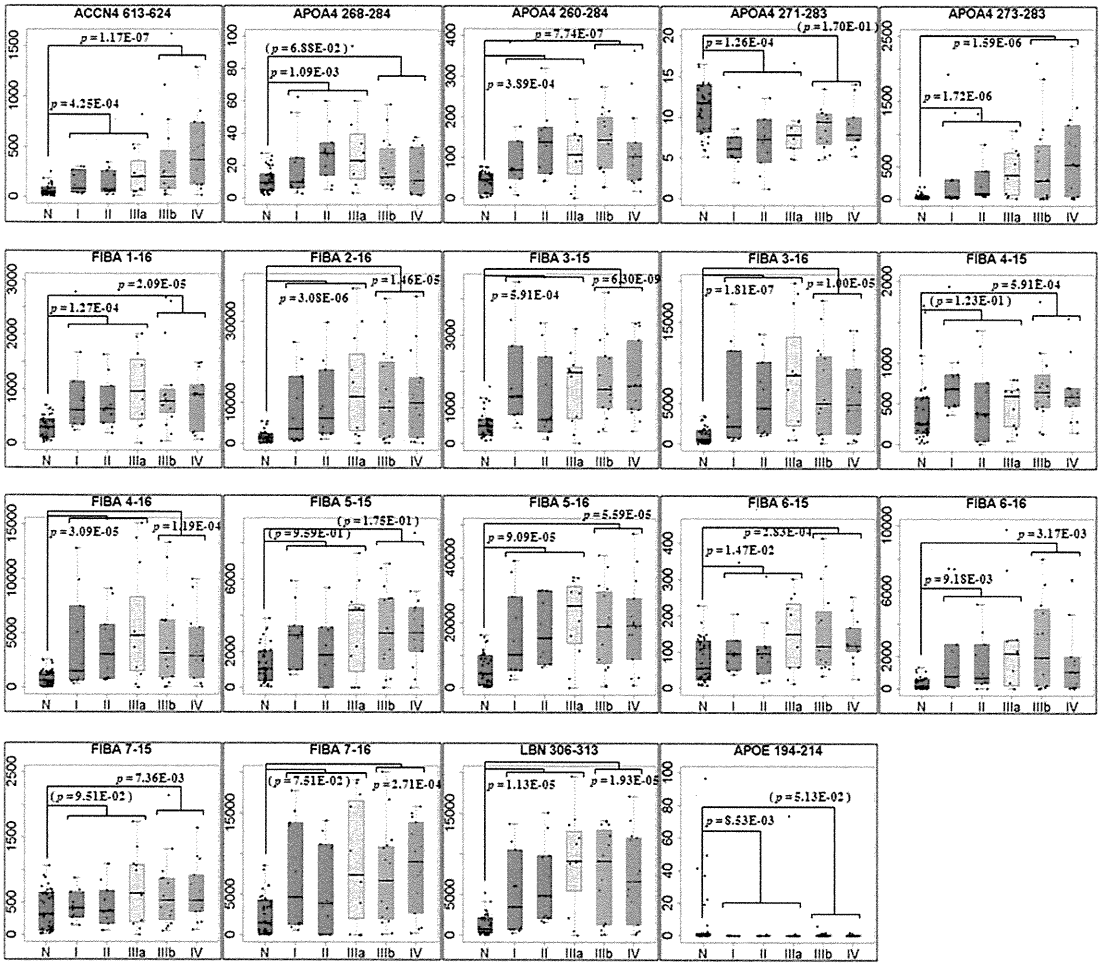
ACCN4 613-624
APOA4 268-284
APOA4 260-284
APOA4 271-283
APOA4 273-283
FIBA 1-16
FIBA 2-16
FIBA 3-15
FIBA 3-16
FIBA 4-15
FIBA 4-16
FIBA 5-15
FIBA 5-16
FIBA 6-15
FIBA 6-16
FIBA 7-15
FIBA 7-16
LBN 306-313
APOE 194-214
N I II IIIa IIIb IV

B

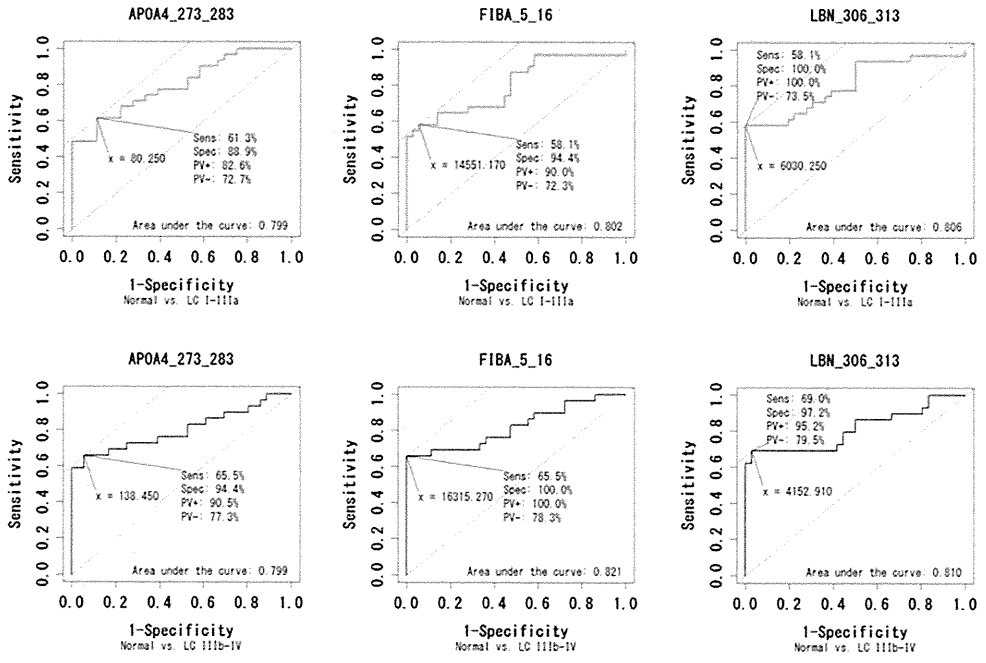
APOA4_273_283
FIBA_5_16
LBN_306_313
Sensitivity
1-Specificity
Area under the curve: 0.799
Area under the curve: 0.802
Area under the curve: 0.806
Area under the curve: 0.799
Area under the curve: 0.821
Area under the curve: 0.810
Normal vs. LC I-IIIa
Normal vs. LC IIIb-IV

Figure 6. Statistical assessment of MRM-based validation experiments. (*A*) Box plots representing the stage-dependent distributions of serum levels of the 19 candidate biomarkers. The p-values from t-test between "normal group (n = 36) and lung cancer stage-I, II, and IIIa (n = 30)" or "normal group (n = 36) and lung cancer stage-IIIb and IV (n = 30)" are shown. The p-values that did not show significant differences were provided in parentheses. N: normal group, I, II, IIIa, IIIb, and IV: lung cancer stage-I, II, IIIa, IIIb, and IV group, respectively. (*B*) ROC curves for APOA4 206–284, FIBA 2–16, and LBN 306–313 were depicted by R. The green or blue graph shows comparison of "normal group (n = 36) and lung cancer stage-I, II, and IIIa (n = 30)" or "normal group (n = 36) and lung cancer stage-IIIb and IV (n = 30)", respectively. The cut-off value was set at the point whose distance from the (sensitivity, specificity) = (1, 1) reached the minimum. The sensitivity (Sens), specificity (Spec), positive predictive value (PV+), negative predictive value (PV-), and area under the curve (AUC) were shown on each graph.
doi:10.1371/journal.pone.0018567.g006

tide A (FPA) which is N terminally cleaved product from fibrinogen α (FIBA). In fact, both our screening and validation results suggested that all of these eight FPA fragments were potential lung cancer-associated biomarkers showing the significant increase of concentrations in lung cancer patients' sera. However, since anomalous turnover of FPA was previously reported in several other diseases including gastric cancer [30], diabetic nephropathy [31], coronary heart disease [32], and others, these 8 FPA fragments could not be defined as lung cancer-specific biomarkers. The other two candidates were generated from apolipoprotein A-IV (APOA4). APOA4 protein itself was already identified as an up-regulated biomarker for ovarian cancer [33], whereas this was also known to be regulated by nutritional and metabolic stress [34]. But both quantitative information and physiological functions of endogenously-processed APOA4 peptides in human serum were still unknown. Interestingly, the APOA4 273–283 fragment demonstrated pathological stage-dependent up-regulation in lung cancer patients' sera, while the two-residue longer fragment APOA4 271–283 was significantly decreased in lung cancer samples (Fig. 6*A*). This indicates the existence of lung cancer-associated endo- or exopeptidases responsible for the cleavage at the C-terminus of APOA4 a.a. 272. Additional two candidate biomarkers, LBN 306–313 and ACCN4 613–624, derived from limbin (LBN) and amiloride-sensitive cation channel 4 (ACCN4) proteins, were reported as cellular membrane proteins. LBN is also known as Ellis-van Creveld syndrome 2 (EVC2) that is expressed in the heart, placenta, lung, liver, skeletal muscle, kidney and pancreas. Defects in LBN (EVC2) are a cause of acrofacial dysostosis Weyers type (WAD, also known as Curry-Hall syndrome) [35]. ACCN4 is a newly identified member of the acid-sensing ion channel family expressed in pituitary gland and weakly in brain [36]. Neither of them was detected in serum previously. Since our study provided the first evidence of LBN 306–313 and ACCN4 613–624 detection in human serum, further analysis of physiological functions and measurement in other diseases should be required for the proper use in clinical lung cancer diagnosis. Hence, the three candidate biomarkers illustrated in Figure 6*B* (APOA4 273–283, FIBA 5–16, and LBN 306–313) were individually considered as clinically useful biomarkers for both early detection and tumor staging of lung cancer, however, integrative measurement of biomarkers such as Figure 4*B* would provide more accurate diagnosis, that could be achievable by MRM-based diagnostic approaches in the future. Consequently the sensitivity of these biomarkers was higher than the currently-used screening biomarker CEA especially at even stage-I or II [8], indicating that new biomarkers addressed in this study had great potential to realize the early detection system for lung cancer. However further validation experiments using high risk groups of lung cancer as the controls (such as heavy smokers or COPD patients) will be necessary to prove the specificity and clinical usefulness of our biomarkers because more practical target population of the early diagnosis of lung cancer should be them rather than healthy individuals.

Finally we grasped the birds-eye view of human peptidome as a snapshot of the specific disease state. We are recently willing to use our peptidome profiling technology to establish an in-house quantitative serum/plasma peptidome database and contribute to the worldwide efforts such as Peptide Atlas (http://www.peptideatlas.org/). This framework would represent a new insight of protease/peptidase activities reflecting a clinical status at a specific time-point of disease and provide essential resources for next-generation extracorporeal diagnostic systems based on mass spectrometry. We therefore hope that researchers at global sites would utilize the peptidome profiling method addressed here and share data to construct mutually beneficial networks and databases which could contribute to the development of future diagnostic technologies worldwide.

Supporting Information

Figure S1 The bar charts illustrating the quantitative screening results for 19 candidates. The normalized peak intensities of 118 candidate biomarker peptides were calculated from 92 serum samples and displayed with bar charts.
(TIF)

Figure S2 MS/MS spectra used for the construction of MRM transitions and peptide identification. All MS/MS spectra were acquired with QSTAR-Elite mass spectrometer in the screening phase (the upper panels). The 1st, 2nd, 3rd, or 4th most intense peaks in each MS/MS spectrum were used for the optimization of MRM transitions (Fig. 5) The middle and the lower panels show the identified fragment ions in MASCOT database search. The ion scores and Expectation values were also indicated in the lower panels.
(TIF)

Figure S3 ROC curves for 19 lung cancer biomarker candidates were depicted by R. The green or blue graph shows comparison of "normal group (n = 36) and lung cancer stage-I, II, and IIIa (n = 30)" or "normal group (n = 36) and lung cancer stage-IIIb and IV (n = 30)", respectively. The cut-off value was set at the point whose distance from the (sensitivity, specificity) = (1, 1) reached the minimum. The sensitivity (Sens), specificity (Spec), positive predictive value (PV+), negative predictive value (PV-), and area under the curve (AUC) were shown on each graph.
(TIF)

Table S1
(DOC)

Table S2
(DOC)

Table S3
(DOC)

Table S4
(DOC)

Acknowledgments

We thank Ms. Mari Kikuchi at AB Sciex for technical assistances.

Author Contributions

Conceived and designed the experiments: KU. Performed the experiments: KU NS ST DK AT. Analyzed the data: KU NS ST AT HN. Contributed reagents/materials/analysis tools: AT YD NI NK KT TS MN T-AS YN HN. Wrote the paper: KU YN HN.

References

1. Parkin DM (2001) Global cancer statistics in the year 2000. Lancet Oncol 2: 533–543.
2. Samet JM, Avila-Tang E, Boffetta P, Hannan LM, Olivo-Marston S, et al. (2009) Lung cancer in never smokers: clinical epidemiology and environmental risk factors. Clin Cancer Res 15: 5626–5645.
3. Goldstraw P, Crowley J, Chansky K, Giroux DJ, Groome PA, et al. (2007) The IASLC Lung Cancer Staging Project: proposals for the revision of the TNM stage groupings in the forthcoming (seventh) edition of the TNM Classification of malignant tumours. J Thorac Oncol 2: 706–714.
4. Henschke CI, Yankelevitz DF, Libby DM, Pasmantier MW, Smith JP, et al. (2006) Survival of patients with stage I lung cancer detected on CT screening. N Engl J Med 355: 1763–1771.
5. Gail MH, Muenz L, McIntire KR, Radovich B, Braunstein G, et al. (1988) Multiple markers for lung cancer diagnosis: validation of models for localized lung cancer. J Natl Cancer Inst 80: 97–101.
6. McCarthy NJ, Swain SM (2001) Tumor markers: should we or shouldn't we? Cancer J 7: 175–177.
7. Brundage MD, Davies D, Mackillop WJ (2002) Prognostic factors in non-small cell lung cancer: a decade of progress. Chest 122: 1037–1057.
8. Sung HJ, Cho JY (2008) Biomarkers for the lung cancer diagnosis and their advances in proteomics. BMB Rep 41: 615–625.
9. Maurya P, Meleady P, Dowling P, Clynes M (2007) Proteomic approaches for serum biomarker discovery in cancer. Anticancer Res 27: 1247–1255.
10. Gamez-Pozo A, Sanchez-Navarro I, Nistal M, Calvo E, Madero R, et al. (2009) MALDI profiling of human lung cancer subtypes. PLoS One 4: e7731.
11. Wollscheid B, Bausch-Fluck D, Henderson C, O'Brien R, Bibel M, et al. (2009) Mass-spectrometric identification and relative quantification of N-linked cell surface glycoproteins. Nat Biotechnol 27: 378–386.
12. Schiess R, Wollscheid B, Aebersold R (2009) Targeted proteomic strategy for clinical biomarker discovery. Mol Oncol 3: 33–44.
13. Ueda K, Takami S, Saichi N, Daigo Y, Ishikawa N, et al. (2010) Development of serum glycoproteomic profiling technique; simultaneous identification of glycosylation sites and site-specific quantification of glycan structure changes. Mol Cell Proteomics 9: 1819–1828.
14. Ostroff RM, Bigbee WL, Franklin W, Gold L, Mehan M, et al. (2010) Unlocking biomarker discovery: large scale application of aptamer proteomic technology for early detection of lung cancer. PLoS One 5: e15003.
15. Villanueva J, Nazarian A, Lawlor K, Tempst P (2009) Monitoring peptidase activities in complex proteomes by MALDI-TOF mass spectrometry. Nat Protoc 4: 1167–1183.
16. Shen Y, Tolic N, Liu T, Zhao R, Petritis BO, et al. (2010) Blood peptidome-degradome profile of breast cancer. PLoS One 5: e13133.
17. Lopez-Otin C, Bond JS (2008) Proteases: multifunctional enzymes in life and disease. J Biol Chem 283: 30433–30437.
18. Overall CM, Blobel CP (2007) In search of partners: linking extracellular proteases to substrates. Nat Rev Mol Cell Biol 8: 245–257.
19. Palermo C, Joyce JA (2008) Cysteine cathepsin proteases as pharmacological targets in cancer. Trends Pharmacol Sci 29: 22–28.
20. Lopez-Otin C, Matrisian LM (2007) Emerging roles of proteases in tumour suppression. Nat Rev Cancer 7: 800–808.
21. Egeblad M, Werb Z (2002) New functions for the matrix metalloproteinases in cancer progression. Nat Rev Cancer 2: 161–174.
22. Albrethsen J, Bogebo R, Gammeltoft S, Olsen J, Winther B, et al. (2005) Upregulated expression of human neutrophil peptides 1, 2 and 3 (HNP 1-3) in colon cancer serum and tumours: a biomarker study. BMC Cancer 5: 8.
23. Sasaki K, Takahashi N, Satoh M, Yamasaki M, Minamino N (2010) A peptidomics strategy for discovering endogenous bioactive peptides. J Proteome Res 9: 5047–5052.
24. Anderson NL, Anderson NG, Pearson TW, Borchers CH, Paulovich AG, et al. (2009) A human proteome detection and quantitation project. Mol Cell Proteomics 8: 883–886.
25. Liu M, Li CF, Chen HS, Lin LQ, Zhang CP, et al. (2010) Differential expression of proteomics models of colorectal cancer, colorectal benign disease and healthy controls. Proteome Sci 8: 16.
26. Qiu FM, Yu JK, Chen YD, Jin QF, Sui MH, et al. (2009) Mining novel biomarkers for prognosis of gastric cancer with serum proteomics. J Exp Clin Cancer Res 28: 126.
27. Wang Q, Shen J, Li ZF, Jie JZ, Wang WY, et al. (2009) Limitations in SELDI-TOF MS whole serum proteomic profiling with IMAC surface to specifically detect colorectal cancer. BMC Cancer 9: 287.
28. Wong MY, Yu KO, Poon TC, Ang IL, Law MK, et al. (2010) A magnetic bead-based serum proteomic fingerprinting method for parallel analytical analysis and micropreparative purification. Electrophoresis 31: 1721–1730.
29. Huang Z, Shi Y, Cai B, Wang L, Wu Y, et al. (2009) MALDI-TOF MS combined with magnetic beads for detecting serum protein biomarkers and establishment of boosting decision tree model for diagnosis of systemic lupus erythematosus. Rheumatology (Oxford) 48: 626–631.
30. Ebert MP, Niemeyer D, Deininger SO, Wex T, Knippig C, et al. (2006) Identification and confirmation of increased fibrinopeptide a serum protein levels in gastric cancer sera by magnet bead assisted MALDI-TOF mass spectrometry. J Proteome Res 5: 2152–2158.
31. Gianazza E, Mainini V, Castoldi G, Chinello C, Zerbini G, et al. (2010) Different expression of fibrinopeptide A and related fragments in serum of type 1 diabetic patients with nephropathy. J Proteomics 73: 593–601.
32. Zito F, Drummond F, Bujac SR, Esnouf MP, Morrissey JH, et al. (2000) Epidemiological and genetic associations of activated factor XII concentration with factor VII activity, fibrinopeptide A concentration, and risk of coronary heart disease in men. Circulation 102: 2058–2062.
33. Dieplinger H, Ankerst DP, Burges A, Lenhard M, Lingenhel A, et al. (2009) Afamin and apolipoprotein A-IV: novel protein markers for ovarian cancer. Cancer Epidemiol Biomarkers Prev 18: 1127–1133.
34. Hanniman EA, Lambert G, Inoue Y, Gonzalez FJ, Sinal CJ (2006) Apolipoprotein A-IV is regulated by nutritional and metabolic stress: involvement of glucocorticoids, HNF-4 alpha, and PGC-1 alpha. J Lipid Res 47: 2503–2514.
35. Galdzicka M, Patnala S, Hirshman MG, Cai JF, Nitowsky H, et al. (2002) A new gene, EVC2, is mutated in Ellis-van Creveld syndrome. Mol Genet Metab 77: 291–295.
36. Grunder S, Geissler HS, Bassler EL, Ruppersberg JP (2000) A new member of acid-sensing ion channels from pituitary gland. Neuroreport 11: 1607–1611.

ORIGINAL ARTICLE

Cytometry
PART A
Journal of the International Society for Advancement of Cytometry

Plasma-Dependent, Antibody- and Fcγ Receptor-Mediated Translocation of CD8 Molecules from T cells to Monocytes

Sari Iwasaki,[1,2] Sakiko Masuda,[3] Tomohisa Baba,[2] Utano Tomaru,[2] Kazuaki Katsumata,[1] Masanori Kasahara,[2] Akihiro Ishizu[1]*

[1]Faculty of Health Sciences, Hokkaido University, Sapporo, Japan

[2]Department of Pathology, Hokkaido University Graduate School of Medicine, Sapporo, Japan

[3]Graduate School of Health Sciences, Hokkaido University, Sapporo, Japan

Received 14 May 2010; Revision Received 19 August 2010; Accepted 21 September 2010

Additional Supporting Information may be found in the online version of this article.

Grant sponsors: Grants-in-Aid for Scientific Research from the Ministry of Education, Culture, Sports, Science and Technology of Japan; Hokkaido University, Faculty of Health Sciences.

*Correspondence to: Akihiro Ishizu, Faculty of Health Sciences, Hokkaido University, Kita-12, Nishi-5, Kita-ku, Sapporo 060-0812, Japan

Email: aishizu@med.hokudai.ac.jp

Published online 28 October 2010 in Wiley Online Library (wileyonlinelibrary.com)

DOI: 10.1002/cyto.a.20984

Abstract

CD8αβ heterodimers are mainly expressed on cytotoxic T lymphocytes. This study demonstrated the detection of CD8αβ heterodimers on human monocytes by whole blood erythrocyte lysis method in flow cytometry. Results revealed that CD8αβ heterodimers were not produced by monocytes themselves, but were transferred from T cells to monocytes when these cells were coincubated in plasma and with anti-CD8 monoclonal antibody (mAb). For completion of CD8 translocation from T cells to monocytes, cell-to-cell contact between T cells and monocytes, as well as binding of the Fc portion of the anti-CD8 mAb and Fcγ receptor II (FcγRII) on monocytes were required. Furthermore, the dynamism of cell membrane and cytoskeleton were involved in the mechanism of CD8 translocation. Interestingly, CD3 and αβT cell receptor (TCR) were also transferred from T cells to monocytes accompanied by CD8. These phenomena are consistent with Ab-dependent and FcγR-mediated trogocytosis, which is recently recognized as one of the intercellular communication processes of the immune system. Trogocytosis means exchange of plasma membrane including cell surface molecules in conjugates formed between immune cells. Results of this study could provide another model of trogocytosis and clearly indicated that putative plasma factors were critically implicated in the mechanism of Ab-dependent and FcγR-mediated trogocytosis. © 2010 International Society for Advancement of Cytometry

Key terms

monocyte; T cell; plasma; Fcγ receptor; trogocytosis

CD8 is a surface glycoprotein mainly expressed on cytotoxic T lymphocytes (CTLs) (1). CD8 functions as a coreceptor that enhances antigen presentation by major histocompatibility complex (MHC) class I to T cell receptors (TCRs). Cell surface CD8 is constituted as either CD8αα homodimer or CD8αβ heterodimer (2). This structural diversity is related to the tissue distribution, ligand specificity, and efficiency on antigen presentation. CD8αβ heterodimers are expressed on the surface of major T lineage cells, including $\alpha\beta TCR^+$ thymocytes and peripheral T cells, whereas CD8αα homodimers are distributed on fewer but broader type of cells, such as $\alpha\beta TCR^+$ and $\gamma\delta TCR^+$ intestinal intraepithelial lymphocytes, natural killer (NK) cells, and dendritic cells (DCs) (3).

We previously reported that CD8αβ heterodimers were expressed on a novel subpopulation of macrophage lineage cells in rat peripheral blood (4). These cells are precursors of $CD8\alpha\beta^+$ macrophages infiltrating into tissues with inflammation. $CD8\alpha\beta^+$ macrophages and the precursors express CD8α and CD8β mRNAs and also molecules with cytotoxic properties, including perforin and granzyme B. $CD8\alpha\beta^+$ macrophages and the precursors with potential cytotoxic property play a pivotal role in the immune system. On the other hand, Gibbings et al. reported that a small number of human monocytes expressed CD8αα homodimers, which enhanced the

ISAC
International Society for Advancement of Cytometry

Fcγ receptor (FcγR)-dependent immune response (5). To the best of our knowledge, the presence of CD8αβ$^+$ human monocytes has not been documented in the literature.

During the search for human counterparts of rat CD8αβ$^+$ macrophages and the precursors, this study discovered CD8α$^+$ monocytes in human peripheral blood by whole blood erythrocyte lysis method in flow cytometry (FCM). In this study, CD8α$^+$ monocytes were designated as CD8$^+$ monocytes. Further studies revealed that CD8 molecules detected on monocytes included CD8αα homodimers and CD8αβ heterodimers. However, contrary to the findings in rats, human CD8$^+$ monocytes weakly expressed the CD8α mRNA and not at all the CD8β mRNA. In addition, human CD8$^+$ monocytes did not express either of the cytotoxic molecules, perforin and granzyme B. These findings suggested that human CD8αβ$^+$ monocytes could possess unique properties but could not function as the counterpart of rat CD8αβ$^+$ macrophages and the precursors.

In this study, the transfer of CD8αβ heterodimers from T cells to monocytes was demonstrated. Further findings included that (1) plasma-dependent CD8 translocation from T cells to monocytes, (2) importance of cell-to-cell contact between T cells and monocytes for CD8 translocation, (3) contribution of the Fc portion of the anti-CD8 monoclonal antibody (mAb) and FcγRII on monocytes, as well as the involvement of dynamism of cell membrane and cytoskeleton, and (4) transfer of CD3 and αβT cell receptor (TCR) from T cells to monocytes accompanied by CD8. Furthermore, it was confirmed that after coculturing monocytes with fluorescence-conjugated anti-CD8-labeled T cells, the fluorescent signal was evident on the monocytes. These phenomena are consistent with Ab-dependent and FcγR-mediated trogocytosis, which is recently recognized as one of the intercellular communication processes of the immune system (6). Trogocytosis means exchange of plasma membrane, cell surface molecules and all, in conjugates formed between immune cells. Our data provides a model of trogocytosis, which can demonstrate the precise mechanism of Ab-dependent and FcγR-mediated trogocytosis.

Materials and Methods

Human Blood Samples

Human blood samples were obtained from healthy volunteers with informed consent. No one had medical history of autoimmune disease, recent infection, or neoplasm.

Antibodies (Abs)

Mouse anti-human monoclonal Abs (mAbs) used were anti-CD3 (UCHT-1, BD Pharmingen, Franklin Lakes, NJ), anti-CD4 (RPA-T4, BD Pharmingen), anti-CD8α (HIT8a, BD Pharmingen), anti-CD8β (2ST8.5H7, Serotec, Oxford, UK), anti-CD14 (M5E2 and MφP9, BD Pharmingen), anti-CD32 (AT10, Abcam, Cambridge, MA), and anti-αβTCR (WT31, BD Pharmingen). IgG1 was the isotype of these mAbs, except for 2ST8.5H7 (IgG2a), M5E2 (IgG2a), and MφP9 (IgG2b). Isotype-matched mouse IgG1 (MOPC-31C, BD Pharmingen), IgG2a (DAK-GO5, Dako, Glostrup, Denmark), or IgG2b (MPC-11, BD Pharmingen) served as control. Alexa488-labeled anti-mouse IgG2a (Invitrogen, Carlsbag, CA) or Alexa488-labeled anti-mouse IgG (H+L) (Invitrogen) was used as secondary Ab for indirect immunostaining.

Fluorescence-Labeling of CD8αβ$^+$ Monocytes in Human Peripheral Blood

Heparinized human peripheral blood was utilized for direct or indirect immunostaining without removal of plasma. For detection of CD8α$^+$ cells in CD14$^+$ monocytes, blood samples (100 μL) were made to react with 0.1 μg of PE-labeled anti-CD8α and FITC-labeled anti-CD14 (M5E2) mAbs for 20 min at room temperature, followed by depletion of erythrocytes by treatment with ammonium chloride as previously described (7). PE-labeled mouse IgG1 and FITC-labeled mouse IgG2a were used as isotype-matched controls for the anti-CD8α and anti-CD14 mAbs, respectively. Next, for detection of CD8β$^+$ cells in CD14$^+$ monocytes, the blood samples (100 μL) were allowed to react with 0.1 μg of unlabeled anti-CD8β mAb or mouse IgG2a for 20 min at room temperature. This was followed by depletion of erythrocytes, and then the cells resuspended in PBS (100 μL) were made to react with 0.04 μg of Alexa488-labeled anti-mouse IgG2a and 0.1 μg of PerCP-labeled anti-CD14 (MφP9) mAbs for 20 min at room temperature. PerCP-labeled mouse IgG2b was used as isotype-matched control for the anti-CD14 mAb. For triple staining of CD8α, CD8β, and CD14, the blood samples (100 μL) were allowed to react with 0.1 μg of unlabeled anti-CD8β mAb or mouse IgG2a for 20 min at room temperature, followed by depletion of erythrocytes, and then the cells resuspended in PBS (100 μL) were made to react with 0.04 μg of Alexa488-labeled anti-mouse IgG2a, 0.1 μg of PE-labeled anti-CD8α, and 0.1 μg of PerCP-labeled anti-CD14 (MφP9) Abs for 20 min at room temperature. PE-labeled mouse IgG1 and PerCP-labeled mouse IgG2b were used as isotype-matched controls for the anti-CD8α and anti-CD14 mAbs, respectively.

Flow Cytometry (FCM)

The fluorescence-labeled cells were assayed, using FACS Calibur (BD Biosciences, Franklin Lakes, NJ) with CellQuest software (BD Biosciences). The FL1, FL2, and FL3 channels were used for detection of FITC/Alexa488, PE, and PerCP, respectively. Unlabeled cells were used to set up the machine. For multiple staining, single fluorescence-labeled cells were used for compensation of the fluorescent levels.

Sorting of CD8$^+$ Monocytes, CD8$^-$ Monocytes, and Lymphocytes

CD8$^+$ monocytes, CD8$^-$ monocytes, and lymphocytes were separated from heparinized human peripheral blood. In brief, blood samples (10 mL) were made to react with 5 μg of PE-labeled anti-CD8α mAb for 20 min at room temperature and then diluted with an equal volume of PBS. Peripheral blood mononuclear cells (PBMCs) were separated, using Ficoll-Paque PLUS (Amersham Biosciences, Uppsala, Sweden) and Leucosep (Greiner bio-one, Solingen, Germany) according to the manufacturer's instructions. The PBMCs were resuspended in 1 mL

of MACS buffer, incubated with 2 μg of CD14 MicroBeads for 20 min at 4°C, and then $CD14^+$ cells were positively selected using the MACS system (Miltenyi Biotech, Bergisch Gladbach, Germany) as previously described (4). At the same time, the negative fraction was collected as lymphocytes. Furthermore, the $CD14^+$ cells resuspended in PBS (100 μL) were allowed to react with 0.1 μg of FITC-labeled anti-CD4 mAb for 20 min at room temperature and then both $CD4^{low}CD8^+$ and $CD4^{low}CD8^-$ cells were sorted as $CD8^+$ and $CD8^-$ monocytes, respectively, using FACS Vantage (BD Biosciences). In this experiment, monocytes were identified as the $CD4^{low}$ population instead of $CD14^+$ cells based on the evidence that human monocytes express CD4 at lower level than $CD4^+$ T cells. Accordingly, the purity of $CD8^+$ or $CD8^-$ monocytes was verified by FACS profiles of CD4 and CD8α.

RT-PCR

Total RNAs were extracted using RNeasy Mini kit (Qiagen, Alameda, CA) according to manufacturer's instructions. Samples were treated with 1 unit/μL of DNase I for 15 min at room temperature to avoid contamination of DNA. The purified RNAs were reverse-transcribed by Superscript III reverse transcriptase (Invitrogen), using oligo-dT primers as previously described (4). The cDNA concentration was estimated by absorbance, and 100 ng of cDNA served as templates. PCR was performed in 25 μL reaction with specific primer pairs (25 μM) listed below; glyceraldehyde-3-phosphate dehydrogenase (GAPDH): 5′-AGCGAGATCCCTCCAAAATC-3′ (sense) and 5′-GGCAGAGATGATGACCCTTT-3′ (antisense), CD3ε: 5′-GT GGACATCTGCATCACTGG-3′ (sense) and 5′-TAGTCTGG GTTGGGAACAGG-3′ (antisense), CD8α: 5′-GCGAGACAGT GGAGCTGAA-3′ (sense) and 5′-GGCTTGTTTTGGGAGAG GTA-3′ (antisense), CD8β: 5′-GGCTGTGGCTCCTCTTGG-3′ (sense) and 5′-ATTTTAGCCTCGCAGGACAG-3′ (antisense), CD14: 5′-GCCTAGACCTCAGCCACAAC-3′ (sense) and 5′-CC AGCGAACGACAGATTGA-3′ (antisense). PCR amplification was performed for 35 cycles of 1 min at 94°C, 1 min at 56°C, and 1 min at 72°C. After the final cycle, the PCR products were incubated at 72°C for 10 min to complete polymerization. The PCR products were run on 1.5% agarose gel containing ethidium bromide.

Plasma Exchange Assay

PBMCs were first separated from heparinized whole blood (3 mL) as described earlier. The PBMCs (1×10^6) were resuspended in PBS (100 μL), made to react with 0.1 μg of PE-labeled anti-CD8α and FITC-labeled anti-CD14 (M5E2) mAbs for 20 min at room temperature, and then served for FCM. PE-labeled mouse IgG1 and FITC-labeled mouse IgG2a were used as isotype-matched controls for the anti-CD8α and anti-CD14 mAbs, respectively. Next, PBMCs and plasma were separated from heparinized whole blood samples (3 mL) exhibiting high proportion of $CD8^+$ monocytes ($CD8^+$ $monocytes^{high}$ donor samples) and low proportion of $CD8^+$ monocytes ($CD8^+$ $monocytes^{low}$ donor samples), and then reciprocal exchange of PBMCs and plasma was done. The PBMCs (1×10^6) from $CD8^+$ $monocytes^{high}$ donor samples were resuspended in 100 μL of the autologous plasma or plasma from $CD8^+$ $monocytes^{low}$ donor samples and incubated for 20 min at 37°C. Similarly, the PBMCs from $CD8^+$ $monocytes^{low}$ donor samples were resuspended in the autologous plasma or plasma from $CD8^+$ $monocytes^{high}$ donor samples and incubated. After all preparations, these cells were made to react with 0.1 μg of PE-labeled anti-CD8α and FITC-labeled anti-CD14 (M5E2) mAbs for 20 min at room temperature and then served for FCM. PE-labeled mouse IgG1 and FITC-labeled mouse IgG2a were used as isotype-matched controls for the anti-CD8α and anti-CD14 mAbs, respectively.

Coculture Assay

PBMCs and plasma were separated from heparinized whole blood (3 mL) as described earlier. The PBMCs resuspended in 1 mL of MACS buffer were made to react with 0.5 μg of CD3 MicroBeads (Miltenyi Biotech) for 20 min at 4°C, and then $CD3^+$ cells were positively selected as T cells using the MACS system. At the same time, the negative fraction was collected and further allowed to react with 0.2 μg of CD14 MicroBeads. After incubation for 20 min at 4°C, $CD14^+$ cells were positively selected as monocytes. The PBMCs (1×10^6) and $CD14^+$ monocytes (1×10^6) were resuspended in 100 μL of the autologous plasma. After incubation for 20 min at 37°C, these cells were made to react with 0.1 μg of PE-labeled anti-CD8α and FITC-labeled anti-CD4 mAbs for 20 min at room temperature, and then served for FCM. PE- or FITC-labeled mouse IgG1 was used as isotype-matched control for the anti-CD8α or anti-CD4 mAb, respectively. Next, monocytes (1×10^5) were mixed with T cells (1×10^6) and cultured in wells of the 24-well plate, or monocytes (1×10^6) in wells of the 24-well plate were cocultured with T cells (1×10^7) in the 0.4 μm pore-sized transwell chamber (BD Falcon, Franklin Lakes, NJ) for 20 min at 37°C. Subsequently, these cells in the wells were resuspended in 100 μL of the autologous plasma, allowed to react with 0.1 μg of PE-labeled anti-CD8α and FITC-labeled anti-CD14 (M5E2) mAbs for 20 min at room temperature, and then served for FCM. PE-labeled mouse IgG1 and FITC-labeled mouse IgG2a were used as isotype-matched controls for the anti-CD8α and anti-CD14 mAbs, respectively.

Preparation of $F(ab')_2$ of Anti-CD8α mAb

$F(ab')_2$ fragments of the anti-CD8α mAb and control mouse IgG1 were generated using Mouse IgG1 Fab and $F(ab')_2$ Preparation kit (Pierce, Rockfold, IL) according to the manufacturer's instructions. In brief, 5 μg of the anti-CD8α mAb and mouse IgG1 were digested with the immobilized ficin in the kit for 24 h at 37°C. The cleaved Fc portion and undigested whole IgG were removed, using the immobilized protein A column. The efficiency of the enzymatic cleavage was verified by SDS-PAGE.

FcγR Blocking Assay

Human monocytes express three types of FcγRs, including FcγRI (CD64), FcγRII (CD32), and FcγRIII (CD16) (8). It is known that FcγRs are different in terms of binding affinity to mouse immunoglobulin subclasses, and that mouse IgG1

shows the highest affinity to FcγRII (CD32) among human FcγRs (9). To determine the contribution of FcγRII (CD32) in the detection of $CD8^+$ monocytes, blocking assay for FcγRII (CD32) was conducted. In brief, heparinized blood samples (100 μL) were preincubated with 3 μg of the anti-CD32 (FcγRII) mAb or mouse IgG1 for 45 min at room temperature, followed by depletion of erythrocytes. The cells resuspended in PBS (100 μL) were made to react with 0.1 μg of PE-labeled anti-CD8α and FITC-labeled CD14 (M5E2) mAbs for 20 min at room temperature and then served for FCM. PE-labeled mouse IgG1 and FITC-labeled mouse IgG2a were used as isotype-matched controls for the anti-CD8α and anti-CD14 mAbs, respectively.

Effect of Cell Membrane Fixation on Detection of $CD8^+$ Monocytes

PBMCs and plasma were separated from heparinized whole blood (3 mL) as described earlier. The PBMCs were fixed for 10 min by 4% paraformaldehyde (PFA) at room temperature, washed with cold PBS three times, and then resuspended in PBS (1.5×10^6/300 μL PBS) (10). Yellow–green carboxylate-modified 1.0 μm latex beads (Sigma-Aldrich, St. Louis, MO) were added to the PBMCs (1.5×10^7 beads/1.5×10^6 PBMCs/300 μL PBS) with or without fixation. After incubation for 90 min at 37°C, the cells were washed with cold PBS three times, and inclusion of yellow–green-labeled beads in PBMCs was analyzed using FACS Calibur. PFA-fixed or nonfixed PBMCs (1×10^6) resuspended in 100 μL of the autologous plasma were allowed to react with 0.1 μg of PE-labeled anti-CD8α and FITC-labeled anti-CD14 (M5E2) mAbs for 20 min at room temperature and then served for FCM. PE-labeled mouse IgG1 and FITC-labeled mouse IgG2a were used as isotype-matched controls for the anti-CD8α and anti-CD14 mAbs, respectively.

Effect of Inhibition of Actin Recruitment on Detection of $CD8^+$ Monocytes

For inhibition of actin recruitment, PBMCs were made to react with 2 μg/mL cytochalasin D (CyD, Sigma-Aldrich) or 0.2% ethanol as vehicle control at nontoxic dose for 30 min at 37°C. Then, OVA-FITC (250 μg/mL, Invitrogen) was added to the PBMCs with or without exposure to CyD for 30 min at 37°C. After washing with cold PBS three times, inclusion of OVA-FITC in PBMCs was analyzed using FACS Calibur. PBMCs (1×10^6) resuspended in 100 μL of the autologous plasma were preincubated with or without 2 μg/mL CyD for 30 min at 37°C, followed by reaction with 0.1 μg of PE-labeled anti-CD8α and FITC-labeled anti-CD14 (M5E2) mAbs for 20 min at room temperature, and then served for FCM. PE-labeled mouse IgG1 and FITC-labeled mouse IgG2a were used as isotype-matched controls for the anti-CD8α and anti-CD14 mAbs, respectively.

Detection of Membrane Fragments Transferred from T Cells to Monocytes

The query if cell surface molecules other than CD8 will translocate accompanied by CD8 from T cells to monocytes was raised. Heparinized blood samples (100 μL) were preincubated with 0.1 μg of unlabeled anti-CD8α mAb or mouse IgG1 for 20 min at room temperature, followed by depletion of erythrocytes, and then resuspended in PBS (100 μL). The cells were made to react with 0.1 μg of PE-labeled anti-CD3 and FITC-labeled anti-CD14 (M5E2) mAbs, or FITC-labeled anti-αβTCR and PerCP-labeled anti-CD14 (MφP9) mAbs for 20 min at room temperature. PE-labeled mouse IgG1, FITC-labeled mouse IgG1, FITC-labeled mouse IgG2a, and PerCP-labeled mouse IgG2b were used as isotype-matched controls for the anti-CD3, anti-αβTCR, anti-CD14 (M5E2), and anti-CD14 (MφP9) mAbs, respectively. Finally, whether prelabeled CD8 molecules on T cells would be transferred to monocytes when these cells were cocultured in plasma was examined. $CD3^+$ T cells and $CD14^+$ monocytes were separated from PBMCs as described earlier. The T cells (1×10^6) resuspended in PBS (100 μL) were made to react with 0.1 μg of PE-labeled anti-CD8α mAb for 20 min at room temperature. After washing with PBS, the T cells mixed with monocytes (1×10^5) were resuspended in 100 μL of the autologous plasma for 20 min at 37°C, followed by reaction with 0.1 μg of FITC-labeled anti-CD14 (M5E2) mAb for 20 min at room temperature, and then served for FCM. PE-labeled mouse IgG1 and FITC-labeled mouse IgG2a were used as isotype-matched controls for the anti-CD8α and anti-CD14 mAbs, respectively.

Results

Detection of $CD8^+$ Monocytes in Human Peripheral Blood Samples

Whole blood samples from healthy volunteers were analyzed by whole blood erythrocyte lysis method in FCM. $CD8\alpha^+$ cells were found in monocytes gated as $CD14^+$ cells in all samples examined ($n = 12$) (4). $CD14^+CD8\alpha^+$ cells were designated as $CD8^+$ monocytes. The rates of $CD8^+$ monocytes in whole monocytes exhibited individual variations ranging from 1 to 40%. $CD8^+$ monocytes were also detected when other mAbs to CD8α were used (data not shown). The representative FACS profile is shown in Figure 1A. In this case, 21.1% of $CD14^+$ monocytes showed positive staining for CD8α. When the remainder of the samples after FCM was observed under the fluorescent microscope, dot-like rather than diffuse fluorescence of CD8α was seen on some $CD14^+$ monocytes (Supporting Information Fig. 1). On the other hand, 12.7% of $CD14^+$ monocytes showed positive staining for CD8β (Fig. 1B). Triple staining for CD8α, CD8β, and CD14 revealed that a part of $CD14^+CD8\alpha^+$ cells was positive for CD8β (Fig. 1C). These findings suggested that CD8 molecules detected on monocytes could include CD8αα homodimers and CD8αβ heterodimers.

Detection of CD8αβ Heterodimers Not Produced by Monocytes

Gibbings et al. demonstrated that a small number of human monocytes expressed CD8αα homodimers (5); however, the expression of CD8αβ heterodimers on monocytes was not reported. To determine if CD8αβ heterodimers

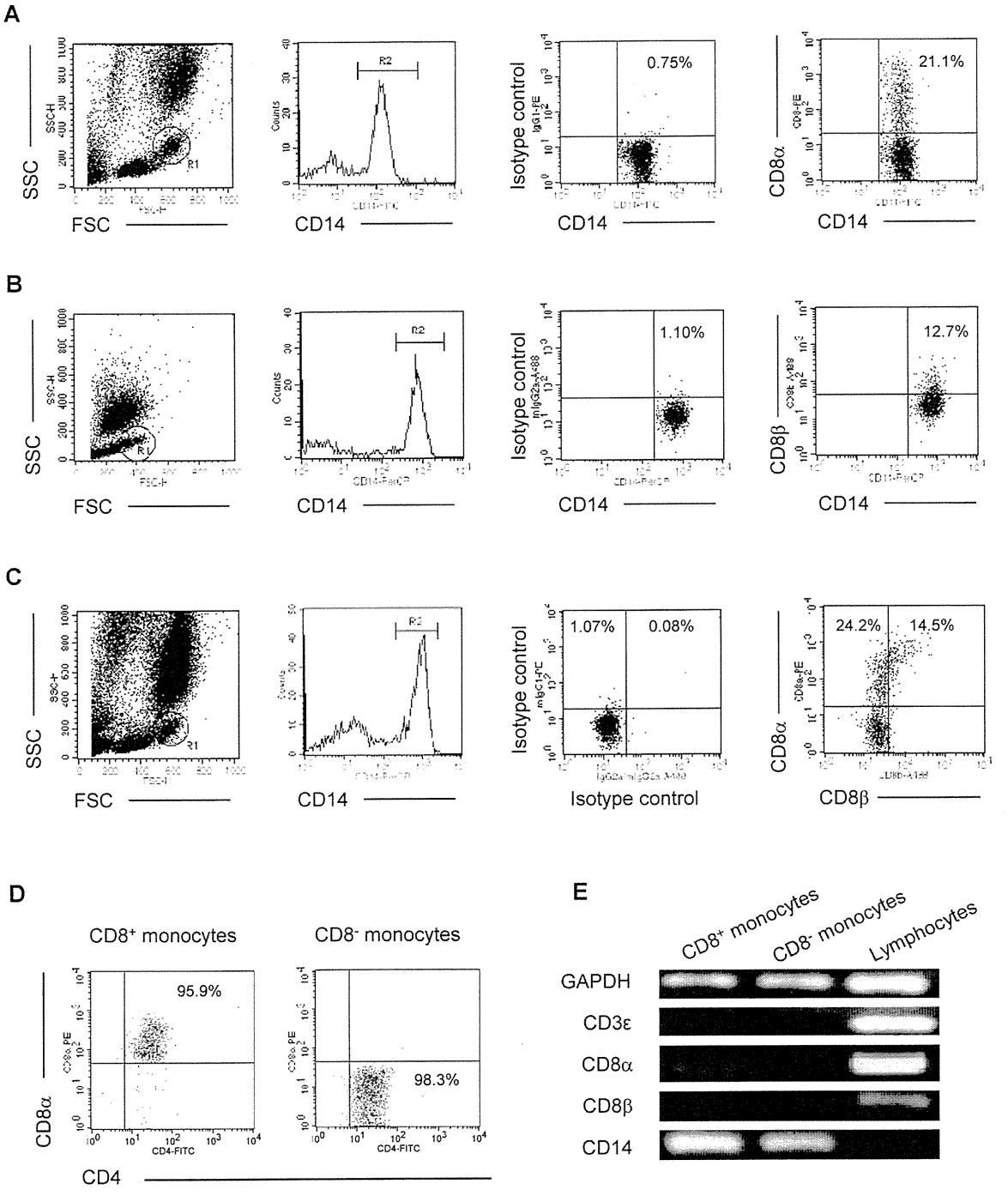

Figure 1. Detection of $CD8^+$ monocytes in human peripheral blood in FCM and lack of expression of the CD8β mRNA in $CD8^+$ monocytes. **A**: Heparinized human peripheral blood samples were allowed to react with PE-labeled anti-CD8α and FITC-labeled anti-CD14 (M5E2) mAbs, followed by depletion of erythrocytes, and then served for FCM. PE-labeled anti-mouse IgG1 and FITC-labeled mouse IgG2a were used as isotype-matched controls for the anti-CD8α and anti-CD14 mAbs, respectively. Cells were divided according to the forward scatter (FSC) and side scatter (SSC) patterns. Monocytes gated in region 1 (R1) and further characterized by high level expression of CD14 (gated in region 2 (R2)) were examined for the expression of CD8α. **B**: The expression of CD8β on $CD14^+$ monocytes was examined. Since fluorescence-labeled anti-CD8β mAb was not commercially available, the CD8β expression was evaluated by the indirect method, using unlabeled anti-CD8β and A488-labeled anti-mouse IgG2a Abs. To label CD14, PerCP-conjugated anti-CD14 (MφP9) mAb was used. Unlabeled mouse IgG2a and PerCP-labeled mouse IgG2b were used as isotype-matched controls for the anti-CD8β and anti-CD14 mAbs, respectively. **C**: Triple staining for CD8α, CD8β, and CD14 was done, using unlabeled anti-CD8β, followed by Alexa488-labeled anti-mouse IgG2a, PE-labeled anti-CD8α, and PerCP-labeled anti-CD14 (MφP9) mAbs. Unlabeled mouse IgG2a, PE-labeled mouse IgG1, and PerCP-labeled mouse IgG2b were used as isotype-matched controls for the anti-CD8β, anti-CD8α, and anti-CD14 mAbs, respectively. Monocytes gated in R1 and further characterized by high level expression of CD14 (gated in R2) were examined for expression of CD8α and CD8β. **D**: The mRNA expression of CD8α and CD8β in $CD8^+$ monocytes was examined by RT-PCR. For this purpose, $CD8^+$ monocytes, $CD8^-$ monocytes, and lymphocytes were separated from whole blood samples as described in the section of "Materials and Methods." The purity of $CD8^+$ monocytes (left panel) and $CD8^-$ monocytes (right panel) was verified by the expressions of CD4 and CD8α in FCM. Since human monocytes express CD4 at a lower level than $CD4^+$ T cells, monocytes were identified as the $CD4^{low}$ population in this experiment. **E**: RT-PCR. The mRNA expressions of CD3ε, CD8α, CD8β, and CD14 were assessed in $CD8^+$ monocytes, $CD8^-$ monocytes, and lymphocytes by 35 cycles of cDNA amplification, using the respective specific primers.